Mon. Not. R. Astron. Soc. **342,** 355–372 (2003)

Correlations between X-ray and radio spectral properties of accreting black holes

Andrzej A. Zdziarski,[1]★ Piotr Lubiński, Marat Gilfanov[2,3] and Mike Revnivtsev[3]

[1]*N. Copernicus Astronomical Center, Bartycka 18, 00-716 Warsaw, Poland*
[2]*Max-Planck-Institut für Astrophysik, Karl-Schwarzschild-Str. 1, 85740 Garching, Germany*
[3]*Space Research Institute, Russian Academy of Sciences, Profsoyuznaya 84/32, 117810 Moscow, Russia*

Accepted 2003 February 19. Received 2003 February 12; in original form 2002 September 18

ABSTRACT

We study correlations between the X-ray spectral index, the strength of Compton reflection, and X-ray and radio fluxes in accreting black holes (Seyferts and black hole binaries). We critically evaluate the evidence for the correlation of the X-ray spectral index with the strength of Compton reflection and consider in detail statistical and systematic effects that can affect it. We study patterns of spectral variability (in particular, pivoting of a power-law spectrum) corresponding to the X-ray index-flux correlation. We also consider implications of the form of observed X-ray spectra and their variability for interpretation of the correlation between the radio and X-ray fluxes. Finally, we discuss accretion geometries that can account for the correlations and their overall theoretical interpretations.

Key words: accretion, accretion discs – radiation mechanisms: thermal – binaries: general – galaxies: Seyfert – X-rays: galaxies – X-rays: stars.

1 INTRODUCTION

X-ray and soft γ-ray (hereafter Xγ) spectra from luminous accreting black holes (hereafter BH), i.e. active galactic nuclei (AGN) and BH binaries, commonly show a distinct component due to Compton reflection (Lightman & White 1988; Magdziarz & Zdziarski 1995) of the primary continuum from a cold medium (e.g. Pounds et al. 1990; Done et al. 1992; Nandra & Pounds 1994; Gierliński et al. 1997; Magdziarz et al. 1998; Weaver, Krolik & Pier 1998; Zdziarski et al. 1998; Zdziarski, Lubiński & Smith 1999, hereafter ZLS99; Życki, Done & Smith 1998, 1999; Gilfanov, Churazov & Revnivtsev 1999, 2000, hereafter GCR00; Revnivtsev, Gilfanov & Churazov 1999, 2001; Done, Madejski & Życki 2000; Eracleous, Sambruna & Mushotzky 2000). A very interesting property of Compton reflection with a number of potential physical implications is that its relative strength, $\sim\Omega/2\pi$, where Ω is the solid angle of the cold reflector as seen from the hot plasma, correlates with some other spectral and timing properties of many sources (e.g. ZLS99; GCR00).

Another correlation often found in both Seyferts and BH binaries is between the X-ray spectral index and the X-ray flux (e.g. Chiang et al. 2000; Done, Madejski & Życki 2000; Nowak, Wilms & Dove 2002; Zdziarski et al. 2002b, hereafter Z02; Gliozzi, Sambruna & Eracleous 2003; Lamer et al. 2003). The X-ray flux is also correlated with the level of radio emission in the hard states of BH binaries (Corbel et al. 2000; Gallo, Fender & Pooley 2002). All of these correlations appear to reflect fundamental properties of BH accretion flows. We critically study the correlations, relationships between them, their theoretical models, and the corresponding physical implications. In Appendix A, we present properties of spectral variability due to a power-law pivoting, which is closely related to the flux-index correlation and it sets constraints on the interpretation of the radio–X-ray correlation. In spectral fits, we use XSPEC (Arnaud 1996).

2 CORRELATION OF COMPTON REFLECTION WITH SPECTRAL INDEX

2.1 Results of fits to data

The first to find a correlation of Compton reflection with another spectral property were Ueda, Ebisawa & Done (1994), who found that Ω correlates with the X-ray photon spectral index, Γ, in the BH candidate GX 339–4, albeit their result was based on only five observations (by *Ginga*). Later, 23 *Ginga* observations of BH and neutron-star binaries were found to obey the same correlation (Zdziarski 1999).

The reality of the correlation has been unambiguously confirmed in the *RXTE* data for the luminous BH binaries Cyg X-1, GX 339–4 and GS 1354–644 (Gilfanov et al. 1999; GCR00; Revnivtsev et al. 2001). Fig. 1 presents those *RXTE* results, as well as the *Ginga* results for 20 observations of Cyg X-1, GX 339–4 and Nova Muscae. These results were mostly obtained with spectra constrained to energies below a few tens of keV. However, in many instances, we also have at our disposal broad-band spectra extending to several hundred keV, where almost the entire range of the reflection

★E-mail: aaz@camk.edu.pl

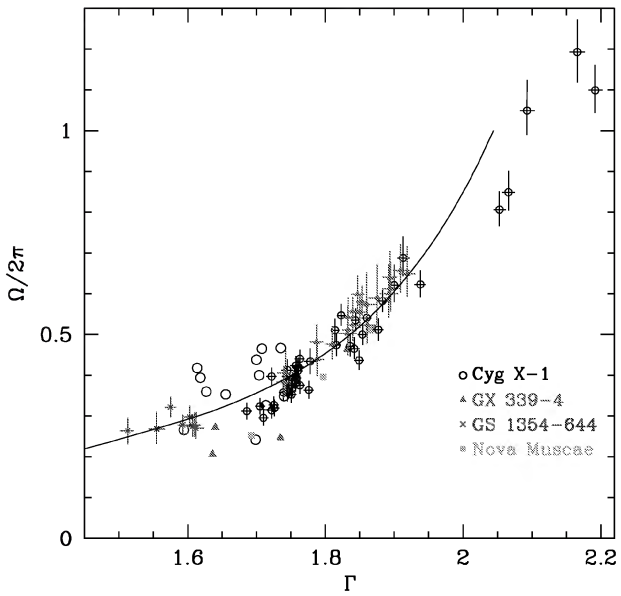

Figure 1. Correlation between the strength of Compton reflection and the X-ray spectral index in BH binaries. Small symbols with error bars and large ones without them correspond to observations by *RXTE* (GCR00 and references therein) and *Ginga* (Zdziarski 1999 and references therein), respectively. The solid curve corresponds to a model of ZLS99 with a central hot source surrounded by an overlapping cold disc.

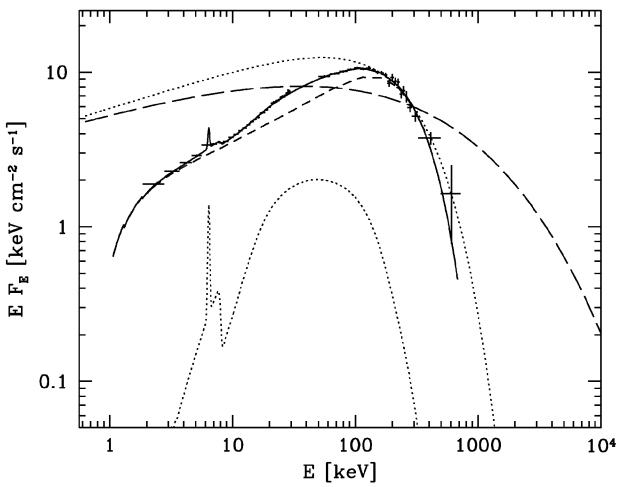

Figure 2. A broad-band $\sim$1–10^3 keV spectrum of Cyg X-1 (Gierliński et al. 1997) fitted by thermal Comptonization and Compton reflection (black solid curve). The two components separately are shown by the short dashes and dots, respectively. At low energies, the spectrum is absorbed in interstellar and circumstellar media. The long dashes and dot/dashes show (unabsorbed) non-thermal synchrotron spectra emitted by power-law electrons with $p = 2.5$ and with an exponential and sharp high-energy cut-off, respectively (see Section 4).

spectrum is found to fit the data very well, together with thermal Comptonization (e.g. the hard states of Cyg X-1, Gierliński et al. 1997, and GX 339–4, Zdziarski et al. 1998), as illustrated in Fig. 2.

The Ω–Γ correlation is also seen in Fourier-resolved spectra, i.e. corresponding to variability in a given range of Fourier frequencies (Gilfanov et al. 1999; Revnivtsev et al. 1999, 2001). Very importantly, the strength of reflection was also found to correlate with the low-frequency quasi-periodic object (QPO) centroid frequency and with the degree of the relativistic smearing of the Fe Kα line (associated with reflection, Życki & Czerny 1994), see fig. 4 in Gilfanov et al. (1999) figs 1.4 and 1.6 in GCR00, fig. 2 in Revnivtsev et al. (2001) and Gilfanov et al. (in preparation).

We note that the above results concern BH binaries in their luminous (and mostly hard) states. Existing data are insufficient to constrain reflection in quiescent states of BH binaries. However, given the prevalent theoretical interpretation of the correlation as being due to feedback between a cold accretion disc and hot plasma (Section 5.1), we do not expect it to be present in quiescence as the disc is then cut-off at a large radius (e.g. Narayan & Yi 1995) and Comptonization of synchrotron photons usually dominates X-rays (e.g. Wardziński & Zdziarski 2000). Analogously, we do not expect an Ω–Γ correlation in low-luminosity AGNs.

The picture of the correlation disappearing with the decreasing luminosity is indeed confirmed in the BH transient GS 2023+338. The results of Życki et al. (1999) show an Ω–Γ correlation in the initial luminous hard state, but then the spectrum substantially softened at an approximately constant Ω when the luminosity decreased by a factor $\gtrsim$10. This effect is most likely to be caused by the onset of the dominance of Comptonization of synchrotron photons with decreasing luminosity (Wardziński & Zdziarski 2000). Similarly, reflection is weak in the transient XTE J1118+480 (Frontera et al. 2001b; Miller et al. 2002), for which the maximum luminosity was only $\sim 10^{-3}$ of the Eddington one.[1]

The first to report an Ω–Γ correlation in an AGN were Magdziarz et al. (1998), in the Seyfert-1 galaxy NGC 5548. Then, ZLS99 showed the presence of a strong Ω–Γ correlation in 47 *Ginga* observations of 23 AGNs (mostly Seyfert 1s and a few intermediate-type AGNs). Matt (2001) presented a compilation of *BeppoSAX* results for Seyfert 1s, and found that Ω is correlated with Γ in the full sample at the confidence level of $>$0.999, and $\sim$0.99 if one object, for which the measurement of the continuum was probably affected by a soft excess, is not taken into account. A similar sample was later studied by Perola et al. (2002, hereafter P02b). Zdziarski & Grandi (2001, hereafter ZG01) showed that Compton reflection in broad-line radio galaxies (also called radio-loud Seyfert 1s), albeit weaker on average than in radio-quiet AGNs, is still consistent with the same correlation. Nandra et al. (2000, hereafter N00) found an Ω–Γ correlation in multiple *RXTE* observations of the Seyfert galaxy NGC 7469. Papadakis et al. (2002, hereafter P02a) have found this correlation in the average properties of four Seyferts. Fig. 3 summarizes those (and some other) results.

It is, however, of importance to consider possible effects that may lead to spurious Ω–Γ correlations. Below, we consider statistical and systematic effects in detail.

2.2 Statistical effects

The main statistical effect is due to the fitted strength of the reflection and the spectral index for a single observation being correlated to a certain degree, resulting in a skewness of their joint error contour. Any data have limited statistics, and then the same intrinsic $\sim$2–20 keV spectrum can be fitted within some confidence limit with either a somewhat harder index and less reflection or a softer index and

[1] An additional complicating factor in measuring reflection in this halo system is its likely overall low metallicity, the possibility of which was considered by Frontera et al. (2001b), but not by Miller et al. (2002), who only considered the case of a low Fe abundance and all other abundances kept at this solar vaule. Thus, the actual value of $\Omega/2\pi$ in this object may still be $\sim$0.2 found by the former authors.

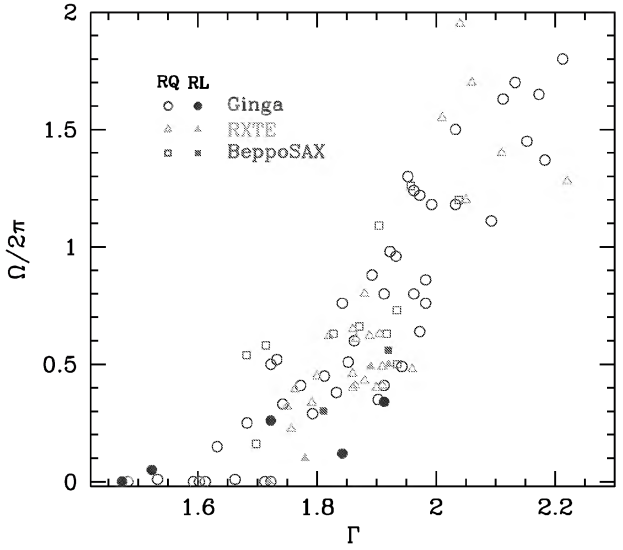

Figure 3. Correlation between the strength of Compton reflection and the X-ray spectral index (in the ∼3–20 keV range, see Section 2.4 and equation [2]) in AGNs. Open and filled symbols correspond to radio-quiet AGNs and active radio galaxies, respectively. Blue circles, green triangles and red squares correspond to observations by *Ginga*, *RXTE* and *BeppoSAX*, respectively. Error bars/contours are not shown for clarity, see Fig. 4(a) for *Ginga* error contours. References for *Ginga*: Lubiński & Zdziarski (2001), Woźniak et al. (1998); *RXTE*: Weaver et al. (1998), Lee et al. (1998), Done et al. (2000), Chiang et al. (2000), P02a, Eracleous et al. (2000), this work (NGC 7469 in Section 2.5); *BeppoSAX*: P02b, Orr et al. (2001), ZG01, Grandi et al. (2001).

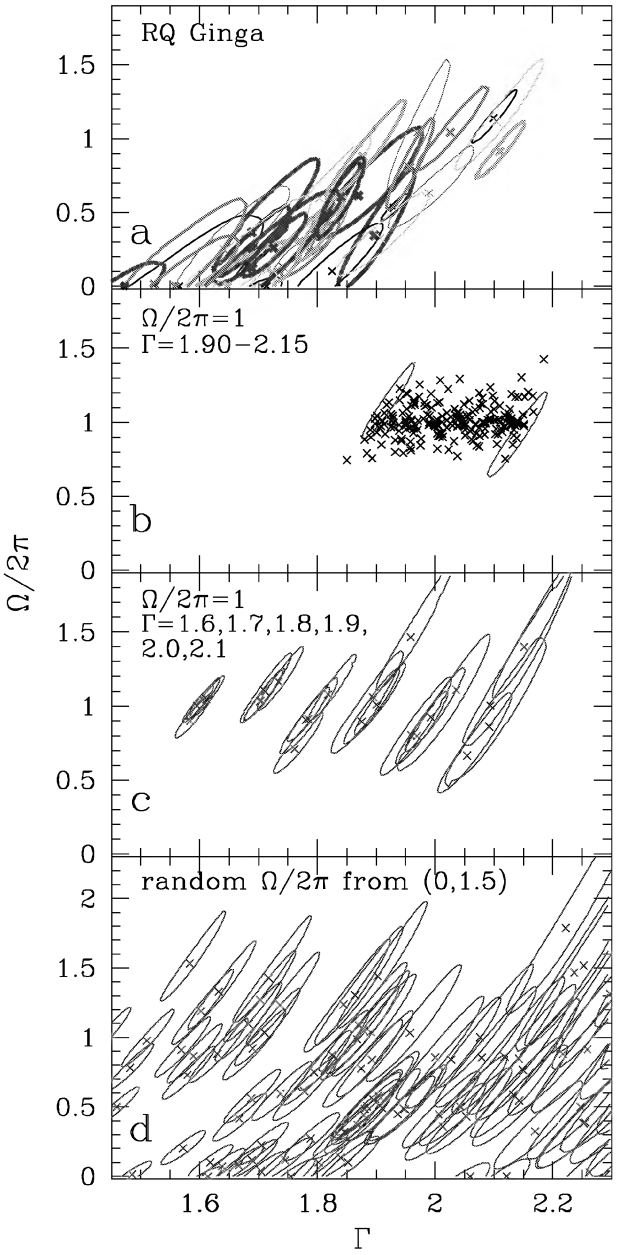

Figure 4. (a) Error contours (1σ for two parameters) for the correlation between Ω and Γ in the *Ginga* data of ZLS99 for AGNs. For clarity of display, only contours with the vertical extent of $\Delta(\Omega/2\pi) < 1$ are shown, and alternating colours and linewidths are used. The panels below show simulations, see the text for details. (b) Best fits and two representative contours for simulated data with a uniform distribution of Γ and fixed Ω. (c) Fixed Ω for six values of Γ. (d) Random Ω for a uniform distribution of Γ. Clearly, all simulation results are very different from the observed distribution.

more reflection. This effect is more important for AGNs than for BH binaries, as the former usually have significantly lower statistics.

As is usual with this type of effect, its importance decreases with increasing statistics. As shown in Fig. 4(a), the extent of typical error contours for Seyferts is *much less* than the global extent of the correlation, and the inclination of an individual contour is also significantly steeper from that of the correlation. Thus, it is already very unlikely that statistical effects alone can account for this distribution.

Then, Vaughan & Edelson (2001, hereafter VE01) considered 120 simulated *RXTE* spectra based on observations of MCG–6-30-15 with short exposure times of ∼1.4–3.7 ks and the top layer of the *RXTE* PCUs 0–2. They used a power-law model with Γ in a relatively narrow range, ∼1.9–2.15 for 90 per cent of the simulated spectra, and constant reflection at $\Omega/2\pi = 1.42$. They fitted the simulated spectra with Γ and $\Omega/2\pi$ as free parameters. The fitted values of (Γ, $\Omega/2\pi$) formed a skewed elongated contour extending from ∼(1.75, 0.5) to ∼(2.3, 3).

Given the assumed narrow range of Γ, the (Γ, $\Omega/2\pi$) contour obtained by them is equivalent (except for some spread in the values of Γ and the exposure time) to the statistical error contour for two parameters. Indeed, the typical error bars provided by VE01 are comparable to the extent of their contour. However, based on the extent of this contour, VE01 stated that the above statistical effect casts serious doubts on the claim of the correlation by ZLS99.

However, most of the error contours of ZLS99 (Fig. 4a) and of those corresponding to *RXTE* and *BeppoSAX* results of Fig. 3 are much smaller than the contour obtained by VE01 due to much better statistics. In particular, the typical statistics in the *Ginga* spectra is an order of magnitude better than those of the one-orbit simulated spectra of VE01. Also, the shape of the error contour of VE01 is significantly different from those observed (Fig. 3). Already based on the above, the suggestion of VE01 is unlikely to be correct.

In order to study this issue quantitatively, we have generated 208 simulated *RXTE* spectra (assuming a 0.5 per cent systematic error, which we estimated from our fits to Crab data) with the range of Γ of 1.90–2.15 (similar to that of VE01) and the constant $\Omega/2\pi = 1$. In the simulations, we have assumed a source with a constant

2–10 keV flux of 3.5 (the flux unit is 10^{-11} erg cm^{-2} s^{-1} hereafter in this paragraph) and an exposure of 50 ks for PCUs 0–2 and 30 ks for PCUs 3–4, similar to that of observations of NGC 7469, see Section 2.5 below. The product of the flux and exposure roughly corresponds to typical *RXTE* measurements shown in Fig. 3. For example, NGC 5548 has flux in the range of ∼5–10, exposures of ∼20–40 ks (Chiang et al. 2000; see also Section 2.5 below), IC 4329A has a flux of ∼15, an exposure of ∼70 ks (Done et al. 2000) and 3C 120 has a flux of ∼6, an exposure of ∼60 ks (Eracleous et al. 2000). The results are shown in Fig. 4(b). We clearly see that the obtained distribution is very different from those in Figs 3 and 4(a). It is also different from the contour of VE01 due to the better statistics.

In Fig. 4(b), we also show two representative error contours. We see that although they correspond to only 1σ, they do provide a good measure of the spread of almost all the simulated points. This overestimate of statistical errors by XSPEC is due to the corresponding overestimate of background errors (added in quadrature to the total ones) discussed by N00 and VE01. In order to account for this effect, N00 did not include background errors in their data at all, and VE01 performed simulations to estimate the actual errors. In the case of the *Ginga* data of ZLS99, the standard XSPEC procedure was followed. Thus, the error contours in Fig. 4(a) are somewhat overestimated. However, this is a conservative approach, which can only *reduce* the measured strength of an actual correlation but will not lead to the appearance of a spurious one. Therefore, we find the suggestion of Edelson & Vaughan (2000) (based on the results of VE01) that the correlation of ZLS99 could be spurious due to inadequate modelling of errors to be incorrect.

The results of simulations with a larger range of the input Γ (and other assumptions similar to those above except for the systematic error now being 0.01) are shown in Fig. 4(c). These results also show how the fitted values of Γ and $\Omega/2\pi$ correlate with those assumed. We see no systematic effects here apart from the dispersion of the fitted value of $\Omega/2\pi$ increasing with increasing Γ (due to decreasing photon statistics at high energies).

To further study possible contributions from statistical effects, we have also performed analogous simulations (using the exposure time, 5.4 ks, and a response as for a *Ginga* observation of NGC 3516[2]) assuming $\Omega/2\pi$ to be random in the 0–1.5 range. Results for 100 simulated spectra are shown in Fig. 4(d). We see that the obtained distribution is still very different from that of Fig. 4(a).

Our results confirm the finding of ZLS99 that the probability of a spectrum with (Γ, $\Omega/2\pi$) measured to be at the high end of the extent of the correlation shown in Fig. 4(a) would correspond in reality to a point at a low end of the correlation is extremely low. ZLS99 noted that (Γ, $\Omega/2\pi$) contours are skewed and elongated (see Fig. 4a), and thus used a statistical method, taking into account the correlated errors while looking for the actual functional dependences between parameters. Based on a comparison of the resulting values of χ^2 (Bevington & Robinson 1992), ZLS99 determined the probability of the correlation appearing by chance as $\sim 10^{-10}$. The exact value may be somewhat different because the model with an allowed $\Omega(\Gamma)$ dependence yields $\chi^2/\nu \sim 2$ (which reflects the intrinsic spread of the data). Still, the probability of reducing χ^2 from 312 (assuming constant Ω) to 115 [allowing for a phenomenological $\Omega(\Gamma)$ dependence as a power law] by chance is in any case $\ll 1$.

[2] The *Ginga* spectra available to us are already background-subtracted, and their errors have been calculated including the uncertainty of the background. On the other hand, simulations give errors neglecting the effect of the background. For this particular source, this results in a decrease of the errors roughly corresponding to an increase of the exposure by a factor of ∼2. Thus, this set of simulations corresponds to the actual exposure of ∼10 ks, which is still half the actual average exposure in the data of ZLS99 of 20 ks. On the other hand, the effect of background errors in XSPEC is generally overestimated (N00, VE01), and thus the present simulations may better represent the actual uncertainties than those in Figs 4(b) and (c).

2.3 Intrinsic spread and small data samples

In Figs 1, 3 and 4(a) we see that apart from the correlation between Ω and Γ, there is also a clear intrinsic spread of the values of those parameters in the observed Γ–Ω space. This spread is caused by varying model assumptions used in the references on which Figs 1 and 3 are based, differences in calibration of different instruments, and, last but not least, fluctuations due to some physical effects (e.g. orientation) superimposed on the overall $\Omega(\Gamma)$ dependence. The last effect is rather common in astrophysics, in which it is very rare that any two quantities are correlated without any influence of other parameters of the system. In the case of BH binaries, we see a full width of $\Delta(\Omega/2\pi) \sim 0.2$ or so for a given Γ, whereas it is ∼0.5 for Seyferts.

Thus, a finding of no Ω–Γ correlation in a small sample cannot be taken as a proof of the lack of it, even if the statistical quality of the data is very good. Furthermore, a sample with poor statistics cannot be considered a basis of a proof for either the presence or the absence of the correlation. For example, the data points for GX 339–4 by Wilms et al. (1999) have such large error bars and so limited a range of Γ and Ω that no statement concerning the correlation can be made at all. In the case of that source, the actual presence of a strong correlation (see Fig. 1) has later been established by Revnivtsev et al. (2001) and Nowak et al. (2002). Then, P02b claimed the Ω–Γ correlation to be relatively weak in their sample of Seyferts. However, the error bars in their data are large enough for their data to permit the actual presence of a strong correlation. The same holds for the similar data set of Matt (2001), who raised the issue of the influence of statistical effects on the $\Omega(\Gamma)$ correlation found by him in the *BeppoSAX* data but presented no calculations to test it.

2.4 Systematic effects

Various systematic effects might affect the best-fitting values of Ω and Γ, and can lead to biased estimates and to contradictions between results obtained by different instruments and using different spectral models. In certain circumstances these effects could potentially lead to the appearance of spurious correlations between parameters. These effects are considered below.

N00 noted that a background subtraction with a systematic relative error with a specific power-law dependence on energy (reaching 0.03 at 20 keV) may produce a spurious Ω–Γ correlation in their *RXTE* data for NGC 7469. However, it is easy to see that this would be the case only if the dominant variability pattern corresponded to a pivot point at low energies, $\lesssim$10 keV. Apart from the specific case of NGC 7469, we show in Section 3 that the typical pivot energy in Seyferts is $\gg$10 keV, which, in turn, would produce an Ω–Γ anticorrelation. Thus, this explanation cannot be general. Also, in Section 2.5 below, we reanalyse the data of N00 with an updated PCA background model and recover the same correlation. Furthermore, we consider it extremely unlikely that the background would be undersubtracted in the same way in AGNs observed by *Ginga*, *BeppoSAX* and *RXTE*.

Then, Weaver et al. (1998), and later P02b and Malzac & Petrucci (2002, hereafter MP02), noted that a correction needs to be made to

account for the high-energy cut-off in the spectra. Namely, the lower the cut-off the fewer incident photons are available for reflection, and then the fitted value of $\Omega/2\pi$ increases. A related important effect not noticed by P02b is the downward curvature of the incident model spectrum (present in the e-folded power law but not necessarily in Comptonization models) being compensated by an increase in the reflection strength. These two effects help to explain the offset between the *Ginga* and *BeppoSAX* results at low values of reflection noticed by Lubiński & Zdziarski (2001), and seen in Fig. 3. On the other hand, P02b note that the resulting correction to Ω cannot by itself remove the presence of the correlation.

We also point out here the existence of an important correction to the X-ray index not taken into account by P02b. It is the difference between the asymptotic low-energy index, $\Gamma_{\rm f}$, of an e-folded power law,

$$\frac{{\rm d}\dot{N}}{{\rm d}E} \propto E^{-\Gamma_{\rm f}} \exp\left(-\frac{E}{E_{\rm f}}\right) \tag{1}$$

(where N is the photon number), and the actual X-ray index between two energies, E_1 and E_2. The latter equals $\Gamma = \Gamma_{\rm f} + \Delta\Gamma$, where

$$\Delta\Gamma = \frac{E_2 - E_1}{\ln E_2/E_1} E_{\rm f}^{-1} \simeq \frac{9}{E_{\rm f}}, \tag{2}$$

and the second equality corresponds to $E_1 = 3$ keV (limiting the range with possible dominance of a soft X-ray excess or effects of ionized absorption) and $E_2 = 20$ keV, used by ZLS99. At $E_{\rm f} = 400$ keV assumed by them, $\Delta\Gamma \simeq 0.02$, which is negligibly small. Thus, the correlation presented in ZLS99 concerns the actual hard X-ray index.

On the other hand, this model fitted to *BeppoSAX* data on Seyferts by P02b (see also Matt 2001) yield generally lower values of $E_{\rm f}$. Then, the fitted values of $\Omega/2\pi$ increase somewhat with respect to those corresponding to fits with no cut-off. For example, for $E_{\rm f} = 160$ keV, the fitted value of Ω increases by $\sim$50 per cent (P02b). However, as pointed out above, the value of the index needs to be corrected as well, with $\Delta\Gamma = 0.06$. In fact, the two points P02b found to disagree with the correlation of ZLS99 both require substantial corrections in Γ. In particular, $E_{\rm f} = 67$ keV fitted by P02b for Mrk 509 yields a rather large $\Delta\Gamma \simeq 0.13$, increasing the 3–20 keV index from $\Gamma_{\rm f} = 1.58$ (P02b) to $\Gamma \simeq 1.71$. Taking into account both corrections (to Ω and Γ) makes the *BeppoSAX* results (Matt 2001; P02b) quite compatible with those from *Ginga* of ZLS99 (see Fig. 1).

Furthermore, we point out that an e-folded power law is actually a very poor model for thermal Comptonization, for which the physical model fits the spectra of Seyferts well at high energies (e.g. Zdziarski, Poutanen & Johnson 2000). For spectral parameters characteristic to both Seyferts and BH binaries, thermal Comptonization has a much sharper cut-off (following an extended, power-law-like part of the spectrum) than that of the e-folded power law. This is illustrated in Figs 5(a) and (b) for two cases approximately spanning the range of parameters of P02b. This further demonstrates that $\Gamma_{\rm f}$ of the e-folded power-law model has no direct physical meaning. The inadequacy of the e-folded power-law model was also noted by MP02, who have found that the sharper cutoffs of the thermal Comptonization spectra lead to increasing the value of Ω being substantially less than that for the e-folded power law.

In conclusion, results of fits with e-folded power laws need to be treated with caution. We also note that Zdziarski et al. (1995) and Gondek et al. (1996) obtained values of $E_{\rm f} \gtrsim 500$ keV for the average Seyfert spectra using data from the *CGRO*/OSSE detector (which affords coverage to significantly higher energies than

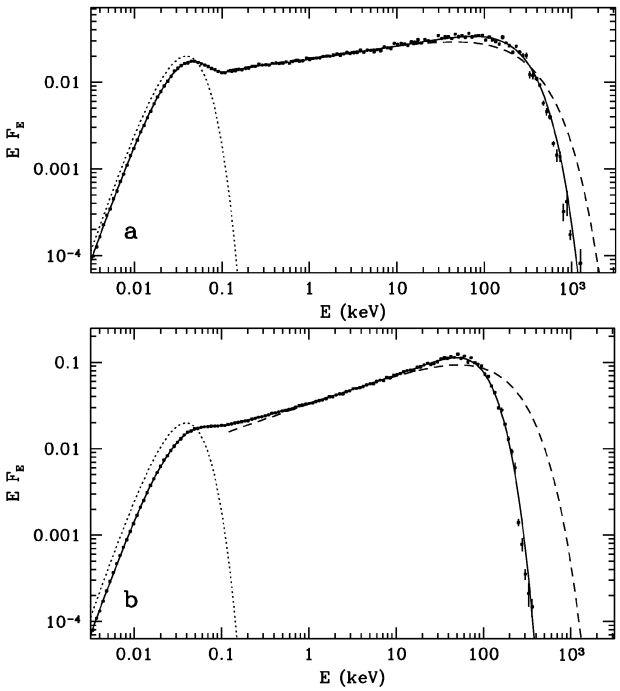

Figure 5. Spectra from isotropic thermal Comptonization compared with e-folded power laws. Blackbody photons with $kT_{\rm bb} = 10$ eV distributed uniformly in a sphere are Comptonized by thermal electrons with the temperature, kT, and the radial Thomson depth, τ. The dotted, solid and dashed curves correspond to the distribution of the input blackbody, Comptonized spectrum calculated by the method of Poutanen & Svensson (1996), and a characteristic e-folded power law with the low-energy index of $\Gamma_{\rm f}$ and the folding energy of $E_{\rm f}$. The filled squares with vertical error bars correspond to Monte Carlo results using the code of Gierliński (2000). The parameters are: (a) $kT = 100$ keV, $\tau = 1$, $\Gamma_{\rm f} = 1.85$, $E_{\rm f} = 300$ keV; (b) $kT = 25$ keV, $\tau = 4$, $\Gamma_{\rm f} = 1.65$, $E_{\rm f} = 150$ keV. We see that in neither case can any e-folded power law approximate the actual spectrum well.

BeppoSAX), i.e. the $E_{\rm f}$ values substantially higher than those from *BeppoSAX*.

In general, there are many other potential systematic effects that can affect the absolute determination of $\Omega/2\pi$, for example, due to an approximate treatment of ionization of the reflecting medium. Then, in order to test the reality of the correlation, we should ask whether a given set of fits properly ranks the spectra by the reflection strength. This issue was addressed by Gilfanov et al. (1999, see their fig. 7) and Revnivtsev et al. (2001, see their fig. 3) in the case of Cyg X-1 and GX 339–4, respectively. They have shown that the *ratio* of the count spectrum fitted with a higher value of $\Omega/2\pi$ to that fitted with a lower value itself has the shape characteristic to Compton reflection. This confirms that fits using relatively simple reflection models do provide a correct ranking in the values of $\Omega/2\pi$.

We would also like to comment on the use of a normalization of the reflection spectrum of Nandra & Pounds (1994) and N00. They characterized the strength of reflection by the 1-keV flux, $A_{\rm ref}$, of a power law with the same Γ as the incident one but normalized to $\Omega/2\pi = 1$. Although equivalent to using the measured $\Omega/2\pi$, this definition may lead to a spurious systematic correlation between $A_{\rm ref}$ and Γ. To illustrate it, let us consider $\Omega/2\pi$ =constant. A common variability pattern of the X-ray power-law spectra of both AGNs and BH binaries is variable Γ with an approximately constant pivot energy, $E_{\rm p}$,

$$\frac{\mathrm{d}\dot{N}}{\mathrm{d}E} = C\left(\frac{E}{E_\mathrm{p}}\right)^{-\Gamma}, \tag{3}$$

where C is the normalization at E_p, and usually $E_\mathrm{p} \gg 1$ keV (see Section 3 below). Then,

$$A_\mathrm{ref} \propto (E_\mathrm{p}/1\ \mathrm{keV})^{\Gamma}, \tag{4}$$

i.e. A_ref is strongly positively correlated with Γ even if the actual reflection solid angle remains constant. Thus, we advise against using this measure of reflection. (We note, however, that the specific data for NGC 7469 of N00 show Γ to be uncorrelated with the X-ray flux, in which case the above effect is not critical and probably does not affect results of that paper substantially.)

2.5 Single objects versus samples

Another issue to bear in mind when considering evidence for and against the Ω–Γ correlation are the distinctions between different classes of sources and between samples of sources and repeated observations of a single source. The evidence for the presence of this correlation in Seyferts was given by ZLS99 mostly for broad-line Seyfert 1s as a class. Repeated observations of single Seyferts give mixed results, sometimes showing the correlation in a given source (e.g. Magdziarz et al. 1998, for NGC 5548; N00 for NGC 7469, also see below), and sometimes not, for example, in IC 4329A (Done et al. 2000) and some other sources (P02b).

Fig. 6(a) shows Ω–Γ contours for *RXTE* observations of the Seyfert 1 NGC 7469 (the inclination was assumed to be $i = 30°$). The data are the same as those of N00, but they have been re-extracted by us using the LHEASOFT 5.2 version of the PCA response matrix and the background model. We used PCUs 0–4 whenever available and grouped the data into 4-d segments, and included a 0.5 per cent systematic error. This yields exposure times of ~50–70 and ~30–50 ks for PCUs 0–2 and 3–4, respectively. The contours clearly show a correlation (which would become even stronger after the reduction of the statistical errors discussed by N00 and VE01, see also Section 2.2). In order to test its reality, we have generated >100 simulated spectra (using the same exposures and fluxes as for the actual data), a selection of them being shown in Fig. 6(b) for two assumed values of Γ. In all cases, we find the statistical $\Omega(\Gamma)$ dependence to be much steeper than the observed one. Thus, we confirm the corresponding conclusion of N00, who also ruled out the origin of the correlation in NGC 7469 from being statistical effects (see their appendix).

Fig. 6(c) shows the results for NGC 5548 from *Ginga* by ZLS99 (contours) and from *RXTE* by Chiang & Blaes (2003) (error bars). Note the good agreement between both sets of measurements after the update of the *RXTE* instrumental response by Chiang & Blaes (2003) with respect to the original result of Chiang et al. (2000), who claimed a disagreement with ZLS99.

In the case of BH binaries, the correlation is seen both in a number of individual objects (Cyg X-1, GX 339–4, Nova Muscae in the hard state) as well as in those sources considered together (Fig. 1). On the other hand, it is certain that there are some BH binaries that do not obey the Ω–Γ correlation. In particular, the disappearance of the correlation with a decreasing Eddington ratio was pointed out in Section 2.1.

Although the data for Cyg X-1 in the soft state lie on the extrapolation of the dependence for the hard state for this and other sources (Fig. 1, see also fig. 5 of Gilfanov et al. 1999), the existing data appear insufficient to conclusively show the presence or absence of the Ω–Γ correlation within the soft state. On the other hand, Rau & Greiner (2003) claimed the presence of an Ω–Γ correlation in relatively soft states of GRS 1915+105. Then, Ballantyne, Iwasawa & Fabian (2001) did not find such a correlation in their sample of five narrow-line Seyfert 1s, which a class of object is likely to be the extragalactic counterpart of the soft state of BH binaries (Pounds,

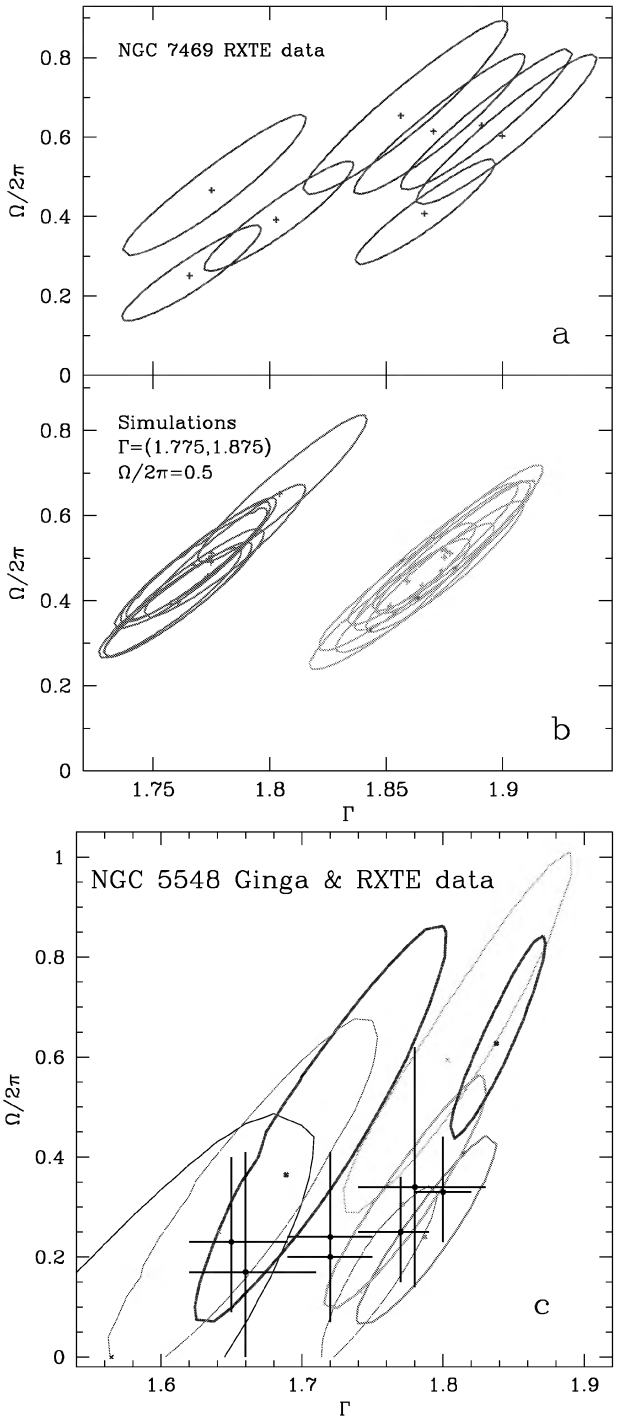

Figure 6. Ω versus Γ in two Seyferts. (a) The 1σ contours for NGC 7469 obtained by us for the *RXTE* data (N00). (b) Simulations for NGC 7469. We confirm the conclusion of N00 that the extent of the correlation cannot be explained by statistical effects. (c) Contours for NGC 5548 from *Ginga* (ZLS99) and error bars from *RXTE* (Chiang & Blaes 2003).

Done & Osborne 1995). Similarly, Lamer et al. (2003) found no Ω–Γ correlation in the narrow-line Seyfert NGC 4051. The lack of correlation in this object may be due to the dominance of the emission process by non-thermal electrons (see Section 5.1), the possibility of which was pointed out by ZLS99 for soft-state sources.

3 X-RAY INDEX-FLUX CORRELATIONS

Another common correlation concerning spectra of accreting BHs is that between the X-ray spectral index, Γ, and the X-ray flux, F. A common situation in the hard state of BH binaries and Seyfert 1s is Γ showing an increasing trend (although often with significant non-statistical scatter) with F in an X-ray energy range, E_1–E_2. Examples of this behaviour are shown in Fig. 7 for the Seyferts

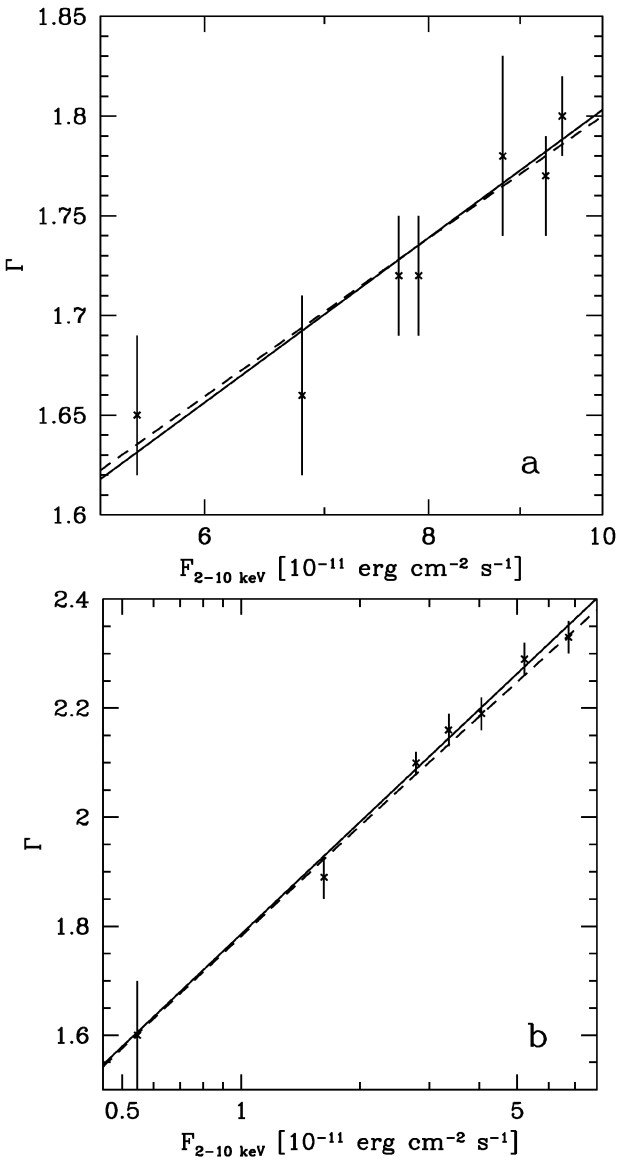

Figure 7. The Γ–F correlation in *RXTE* observations of (a) NGC 5548 and (b) NGC 4051. The data are from Chiang & Blaes (2003) and Lamer et al. (2003), respectively. The solid lines show the best-fitting linear dependence, and the dashed lines show the dependence predicted by equation (7) with $E_p = 180$ and 140 keV, respectively.

NGC 5548 (Chiang & Blaes 2003) and NGC 4051 (Lamer et al. 2003). The Γ–F dependence can often be fitted by a power law (e.g. Chiang et al. 2000; Done et al. 2000), also for the data shown in Fig. 7. The linear dependences of Γ(log F) in Fig. 7 yield $\chi^2/\nu < 1$, i.e. the departures from the linear correlation are compatible with being statistical only. On the other hand, the assumption of a constant Γ results in $\chi^2/\nu = 25/6$ and 138/6, respectively, and the F-test (Bevington & Robinson 1992) yields the probability that the fit improvement is by chance of $\sim 10^{-3}$ and $\sim 10^{-5}$, respectively. Thus, the Γ–F correlations are highly significant statistically, which is also confirmed by application of the Spearman and Kendall rank correlation tests. Similar power-law correlations are found, for example, in the hard state of Cyg X-1 on long time-scales (Z02).

If the index increases from Γ_h to Γ_s while the energy flux increases from F_h to F_s, the two power laws intersect at the pivot energy,

$$E_p = E_1 \left[\frac{F_s}{F_h} \left(\frac{2-\Gamma_s}{2-\Gamma_h} \right) \frac{(E_2/E_1)^{2-\Gamma_h} - 1}{(E_2/E_1)^{2-\Gamma_s} - 1} \right]^{1/(\Gamma_s - \Gamma_h)}, \quad (5)$$

with the following substitution if either Γ equals 2:

$$\frac{(E_2/E_1)^{2-\Gamma} - 1}{2-\Gamma} \rightarrow \ln \frac{E_2}{E_1}. \quad (6)$$

If F_s/F_h represents the ratio of the photon, rather than energy, fluxes, then $2-\Gamma$ above should be replaced everywhere by $1-\Gamma$. The resulting variable power law is given by equation (3). A treatment of the effect of pivoting on average spectra and spectral variability is given in Appendix A.

In the cases of the data for NGC 5548 and 4051, $E_p \simeq 180$ and 140 keV, respectively. As shown in Appendix A, the assumption of a constant E_p results in an almost linear dependence between Γ and the logarithm of the flux over some energy band. Indeed, the E_1–E_2 energy flux, given by

$$F_{E_1-E_2} = C E_p^{\Gamma} \frac{E_2^{2-\Gamma} - E_1^{2-\Gamma}}{2-\Gamma}, \quad (7)$$

and plotted as dashed lines in Fig. 7, almost coincides with the best-fitting linear dependences.

Table 1 gives a number of examples of the pivot energy in Seyferts, as well as in Cyg X-1 and Cyg X-3. Table 1 is based mostly on figures in published papers, and thus the numbers there are approximate only. Still, they unambiguously show that many Seyferts have the pivot energy at $\gg 10$ keV. A similar pattern is shown by MCG–5-23-16 (Zdziarski, Johnson & Magdziarz 1996). Although variable X-ray absorption may affect the correlation for NGC 4151 found by Yaqoob et al. (1993), the weak variability found above 50 keV (Zdziarski et al. 1996; Johnson et al. 1997) is consistent with the pivot at high energies.

Table 1 gives two examples of AGNs with the pivot at $\leqslant 10$ keV, 3C 120 and Mrk 766. In the cases of 3C 120 and Cyg X-1 in the hard state (where the seed photon energies are much higher than those in AGNs, which results in the pivot energy being higher than that in 3C 120, see Z02), ZG01 and Z02 have shown that the spectral variability is consistent with the bolometric luminosity of the high-energy source being constant. This type of behaviour may also take place in the Seyfert 1H 0419–577, where $E_p \sim 7$ keV (see fig. 3 in Page et al. 2002). However, Table 1 shows that this type of behaviour is certainly not the rule. The pivot at high energies implies that the bolometric luminosity increases with the softening of the source, as illustrated in Fig. 8. This is also confirmed by the 1–300 keV luminosity estimated by P02a for MCG–6-30-15, NGC 5506 and

Table 1. Pivoting in accreting black holes.

Object	$E_1 - E_2$ (keV)	Γ_h	Γ_s	F_s/F_h^a	E_p (keV)	Reference
Cyg X-1 (hard state)	3–12	1.4	2.0	3	40[b]	Z02
Cyg X-3 (hard state)	3–100	NA	NA	NA	∼20[c]	McCollough et al. (1999b)
3C 120	0.3–2	1.70	2.03	2[d]	5	ZG01
3C 390.3	1–10	1.70	1.90	1.8[e]	90	Woźniak et al. (1998)
3C 390.3	2–10	1.61	1.79	2.1	300	Gliozzi et al. (2003)
IC 4329A	2–10	1.90	2.07	1.9	200	Done et al. (2000)
IC 4329A	2–10	1.75	1.95	2.2	240	Madejski, Done & Życki (2001)
MCG–6-30-15	2–10	1.8	2.2	3.3[d]	80	VE01
MCG–6-30-15	3–10	1.9	2.2	3.8[f]	410	P02a
Mrk 766	1–10	1.64	2.01	1.5[e]	10	Leighly et al. (1996)
NGC 3227	2–10	1.49	1.75	1.4	20	Ptak et al. (1994)
NGC 3516	2–10	1.63	1.69	1.37	910	Chiang (2002)
NGC 4051	3–10	1.3	2.6	26[f]	60	P02a
NGC 4051	2–10	1.60	2.33	12.3	140	Lamer et al. (2003)
NGC 4151	2–10	1.4	1.7	6	2000	Yaqoob et al. (1993)
NGC 5506	3–10	1.9	2.1	4[f]	5000	P02a
NGC 5548	2–10	1.65	1.80	1.73	180	Chiang & Blaes (2003)
NGC 5548	3–10	1.8	2.0	3.2[f]	1700	P02a

Notes. [a]Energy flux ratio, except when noted. [b]Also observed in the broad-band, 1.5–300 keV, variability (Z02). [c]Implied by the 3–100 keV variability. [d]Count rate ratio assumed here to represent the photon flux ratio. [e]Calculated using the 1-keV normalization. [f]The (3–5)+(7–10) keV count rate ratio assumed here to approximate the 3–10 keV photon flux ratio.

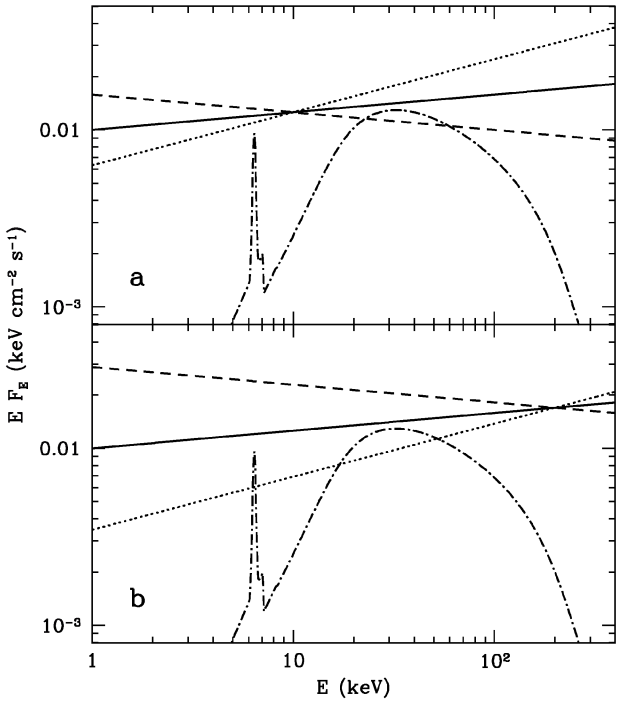

Figure 8. Schematic illustration of power-law spectra with $\Gamma = 1.7$, 1.9 and 2.1 pivoting at (a) $E_p = 10$ keV and (b) $E_p = 200$ keV. The two cases correspond to the total X-ray luminosity being approximately constant and increasing with increasing Γ, respectively. The dot-dashed curve shows a possible constant reflection component from a distant medium. If the total spectrum is fitted by a power law and reflection, the relative reflection fraction will increase and decrease with increasing Γ in cases (a) and (b), respectively.

5548 to increase by a factor of ∼3 for Γ increasing within the ranges given in Table 1. A similar increase is shown for NGC 5548 in fig. 6(a) of Magdziarz et al. (1998). The results of Nowak et al. (2002, see their table 1 and fig. 3) imply that the bolometric luminosity is increasing with the increasing 3–9 keV flux in the hard state of the BH binary GX 339–4. Some increase of the bolometric luminosity with increasing Γ is also found in Cyg X-1 as the source becomes close to a transition to the soft state (Z02).

In the case of MCG–6-30-15, Shih, Iwasawa & Fabian (2002) have found a Γ–F correlation in *ASCA* data to appear to saturate above a certain count rate. They have interpreted this behaviour as being due to a superposition of two power-law components with constant indices, and the normalization of the softer power law was allowed to vary. This model also allows one to explain an approximate constancy of the Fe Kα line flux with varying continuum flux in those data. Thus, this is an attractive model for MCG–6-30-15. On the other hand, data for many objects clearly show correlated hardness changes over rather broad bands (see the references above, for example, P02a), which also rules out the above interpretation as being general. Furthermore, the apparent saturation at high F seen by Shih et al. (2002) (and Merloni & Fabian 2001, hereafter MF01) might be an artefact of plotting Γ against the linear flux[3] rather than $\log F$. As discussed above (see also Appendix A), variability with a constant pivot energy results in a linear dependence between Γ and $\log F$, not F itself. Indeed, the non-linearity and saturation of Γ in NGC 4051 claimed by Lamer et al. (2003) is specific to

[3]Often, the ratio of instrument counts in two bands (the hardness ratio) is plotted as a function of a count rate. The advantages of this choice are independence of possible revisions of the instrument response (giving the conversion between counts and photons), for which revisions are relatively common in X-ray astronomy, and no need to assume a spectral model. Another choice is to plot the fitted spectral index against the fitted energy flux. Although both quantities depend on the response, the advantage of this choice is the ease of comparison with physical models. On the other hand, VE01, MF01 and Shih et al. (2002) show hybrid plots with the fitted Γ against the instrumental count rate. The latter two papers show a comparison of the results with a physical model by MF01 assuming the X-ray count rate to be proportional to the energy flux. This is obviously not strictly correct for a variable X-ray slope, possibly leading to inaccuracies in comparing data with theory.

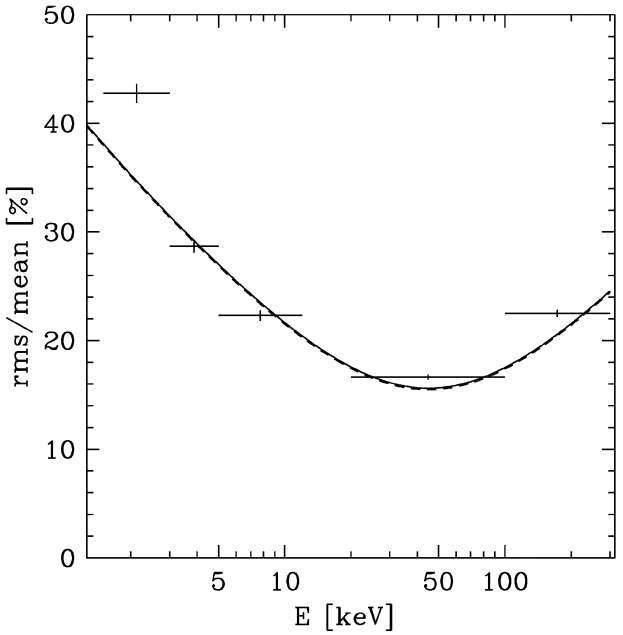

Figure 9. The rms variability in the hard state of Cyg X-1 in 1-d averaged measurements by the *RXTE*/ASM and *CGRO*/BATSE (Z02). The data (crosses) can be modelled by either a power-law pivoting of equation (A6) with $E_p = 45$ keV, the standard deviation of $\Delta_\Gamma = 0.23$, and an additional E-independent variability with $\sigma_0 = 0.155$ (dashed curve), or a variable pivot energy (equation A13) with $E_p^0 = 45$ keV, $\Delta_p = 0.71$ and $\Delta_\Gamma = 0.21$ (solid curve, almost coincident with the dashed one). Note that the non-zero value of the minimum rms of the latter model is entirely due to the dispersion of E_p, see Appendix A.

using a $\Gamma(F)$ plot, and it disappears completely in a $\Gamma(\log F)$ space (Fig. 7b).

An important example of broad-band pivoting variability is given by $\sim 10^3$ of 1-d measurements of Cyg X-1 in the hard state over the 1.5–300 keV energy range (Z02). Pivoting is seen here directly in the ASM and BATSE data showing a linear $\Gamma(\log F)$ correlation at low energies and an anticorrelation at high energies, not just inferred from a Γ–F plot. The pivoting variability pattern can also be illustrated by energy-dependent fractional variability. The solid and dashed curves in Fig. 9 show that the observed fractional rms variability as a function of energy is well modelled by the theoretical rms due to a variable Γ with either constant E_p and additional energy-independent variability or variable E_p. We also see that an additional variable component is required at the lowest energies, which probably can be identified with the observed soft X-ray excess (Ebisawa et al. 1996; Di Salvo et al. 2001; Frontera et al. 2001a). Still, the 1.5–3 keV flux remains strongly anticorrelated with the 100–300 keV flux (Z02).

Results for Seyfert 1s similar to that shown in Fig. 9 for Cyg X-1 have been obtained by Markowitz & Edelson (2001). They show that the fractional variability in the 2–4 keV band in all nine Seyfert 1s studied by them is higher than that in the 7–10 keV band (for long-term measurements with 5-d intervals). Given the unknown shape of the dependence of rms on E, it is not possible to uniquely translate their results into the pivot energies. Still, their results are compatible with $E_p \gtrsim 10$ keV.

The results above were obtained on time-scales from days to years for both Seyferts and BH binaries in the hard state. Interestingly, the variability patterns in the two cases appear qualitatively similar. However, a month time-scale in Seyferts corresponds to $\sim$1 s in BH binaries in units of the light traveltime across the gravitational radius. Thus, the variability pattern presented here for AGNs corresponds physically to that on short-time scales in BH binaries. In agreement with this correspondence, Li, Feng & Chen (1999) find the 2–60 keV hardness to be anticorrelated with the flux (i.e. corresponding to a positive Γ–F correlation) in the hard state of Cyg X-1 at time-scales of 10^{-3} and 1–50 s. Thus, pivoting with a high pivot energy is likely to take place in the BH binaries on short time-scales as well. On the other hand, the full picture of variability in the hard state is certainly more complicated that this. For example, Li et al. (1999) and Wen, Cui & Bradt (2001) find no or weak Γ–F correlation in Cyg X-1 on the 0.01–0.1 s and $\sim$1-d time-scales, respectively, whereas it is very strong over hundreds of days (Z02).

Then, spectral state transitions change the character of the correlation qualitatively. In particular, the Γ–F correlation becomes strongly negative in the soft state of Cyg X-1 over time-scales from 0.01 s to tens of days (Li et al. 1999; Wen et al. 2001; Z02).

4 CORRELATION BETWEEN THE X-RAY AND RADIO FLUXES IN BH BINARIES

A very interesting correlation between radio and X-ray fluxes in the hard state of accreting BH binaries has been discovered recently (Brocksopp et al. 1999; Corbel et al. 2000; Gallo et al. 2002; Markoff et al. 2002). In particular, Gallo et al. (2002) show a strong correlation between the 15-GHz flux and the count rate from the ASM from daily measurements for eight BH binaries in the hard state. There are two possible origins of this correlation. One is that the level of X-ray emission is related to the rate of ejection of radio-emitting clouds, forming a compact jet (e.g. Mirabel et al. 1998; Corbel et al. 2000). Another is that the X-ray emission of BH binaries is dominated by non-thermal emission of the jet (Markoff, Falcke & Fender 2001; Markoff et al. 2002, 2003; Vadawale, Rao & Chakrabarti 2001; Georganopoulos, Aharonian & Kirk 2002).

There are many strong arguments against the second interpretation (see also Poutanen & Zdziarski 2002). The broad-band Xγ spectra of BH binaries in the hard state are very well modelled by thermal Comptonization and Compton reflection (e.g. Gierliński et al. 1997; Zdziarski et al. 1998; Frontera et al. 2001a,b; Wardziński et al. 2002; Z02), see Fig. 2. Apart from those broad-band studies, the evidence for the presence of Compton reflection from X-rays alone is extremely strong (e.g. Gilfanov et al. 1999; CGR00; Revnivtsev et al. 2001; Nowak et al. 2002). This implies that the X-ray emission is not strongly beamed away from the disc.

The thermal-Compton origin of the primary X-ray emission is strongly supported by a remarkable uniformity of both the energy (within a factor of $\sim$2) and shape of the high-energy cutoffs of BH binaries in the hard state observed by OSSE (Grove et al. 1998). This cut-off is naturally accounted for by thermostatic properties of thermal Comptonization and $e^\pm$ pair production (e.g. Malzac, Beloborodov & Poutanen 2001), as it corresponds to the transition to relativistic temperatures. At higher temperatures, cooling becomes extremely efficient and copious pair production starts. This reduces the energy available per particle, causing the temperature to decrease.

Within the framework of the model with synchrotron emission of non-thermal electrons accelerated in the first-order Fermi process in a shock, the maximum energy of the synchrotron photons is given by the balance of the acceleration and energy loss time-scales. This gives the critical synchrotron energy corresponding to the maximum

Lorentz factor of the accelerated particles, $\Gamma_{\rm max}$, as

$$E_{\rm c,max} = \frac{m_{\rm e}c^2}{\alpha_{\rm f}} \frac{3^4 \sin\alpha}{2^5} \frac{\beta_{\rm sh}^2}{\xi}, \quad (8)$$

where $\beta_{\rm sh}c$ is the shock velocity, ξ (satisfying $1/\beta_{\rm sh} \gtrsim \xi \gtrsim 1$) gives the efficiency of the shock acceleration, $\alpha_{\rm f}$ is the fine-structure constant, α is the pitch angle (with $\langle \sin\alpha \rangle \sim \frac{1}{2}$) and $m_{\rm e}\,c^2$ is the electron rest energy. We see that for $\beta_{\rm sh}^2/\xi \sim 10^{-3}$ we can reproduce the high-energy cut-off of BH binaries at $\sim$100 keV, as pointed out by Markoff et al. (2001).

However, even with the fine-tuning of $\beta_{\rm sh}^2/\xi$, the cut-off in the electron distribution is unlikely to be sharp. One effect is that of electron energy loss, which makes the steady-state distributions cut off gradually (e.g. Kirk, Rieger & Mastichiadis 1998). Also, the conditions in the accelerating region (determining the efficiency parameter, ξ) are unlikely to be completely uniform. Under many astrophysical circumstances, the shape of the tail of a distribution is given by an exponential cut-off (e.g. in a Maxwellian). If we assume the power-law electrons, $N(\gamma) = D\gamma^{-p}$, are cut-off as $\exp(-\gamma/\gamma_{\rm max})$, the resulting synchrotron spectrum, $F_E = E\,{\rm d}\dot{N}/{\rm d}E$, is given by

$$F_E = K \left(\frac{E}{E_0}\right)^{(1-p)/2} \int_0^\infty {\rm d}y\, y^{(1+p)/2} {\rm E}_{2+p}\left(\sqrt{\frac{\epsilon}{y}}\right) {\rm K}_{5/3}(y), \quad (9)$$

where $\epsilon = E/E_{\rm c,max}$, $\rm E_{\it n}$ is the exponential integral of the order n, $\rm K_{\it n}$ is the modified Bessel function of the second kind, the normalization constant is

$$K = \frac{\sqrt{3} e^3 B D \sin\alpha}{h m_{\rm e} c^2}, \quad (10)$$

where B is the magnetic field strength, e is the electron charge, h is the Planck constant and E_0 is the constant factor in the critical synchrotron energy, $E_{\rm c}$, corresponding to emission by electrons with the Lorentz factor Γ,

$$E_{\rm c} = E_0 \gamma^2, \quad E_0 = \frac{3 e h B \sin\alpha}{4\pi m_{\rm e} c}. \quad (11)$$

The spectrum of equation (9) exhibits a rather gradual cut-off, in fact *much* more gradual than that of a typical hard-state spectrum of Cyg X-1, as illustrated in Fig. 2. Indeed, the synchrotron model of the hard state of Cyg X-1 shown in fig. 3(a) in Markoff et al. (2002) overestimates the 1-MeV flux (McConnell et al. 2002) by a factor of 8 when matched to its 100-keV flux.

We have also studied various other forms of the electron high-energy cut-off. We have found that anything more gradual than a sharp cut-off at $\Gamma_{\rm max}$, when

$$F_E = \frac{2K}{p+1} \left(\frac{E}{E_0}\right)^{(1-p)/2} \int_\epsilon^\infty {\rm d}y \left[y^{(1+p)/2} - \epsilon^{(1+p)/2}\right] {\rm K}_{5/3}(y), \quad (12)$$

gives photon spectra with cutoffs that are not strong enough to match the cut-off of Cyg X-1, as illustrated in Fig. 2.

A related issue is the spectral index of the spectrum. The model of Markoff et al. (2001) relies on particle acceleration in shocks. As they note, the accelerated electrons then have a power-law index $>$1.5, where 1.5 corresponds to highly relativistic shocks. As the terminal bulk motion of jets in BH binaries is only mildly relativistic, with a typical bulk Lorentz factor of a few, it is unlikely that a shock close to the base of a jet would be highly relativistic. Electron energy losses steepen the steady-state electron distribution by unity (e.g. Kirk et al. 1998), to an index $p > 2.5$, and the corresponding photon index is $\Gamma = (p + 1)/2$. Markoff et al. (2001) have been able to fit this model to the spectrum of XTE J1118+480, which has $\Gamma \simeq 1.8$. However, many BH binaries have X-ray spectra harder than that (see Fig. 1). The resulting discrepancy is illustrated in Fig. 2, where we assumed the limiting $p = 2.5$ in the synchrotron model spectra shown.

In order to deal with this rather serious problem, Markoff et al. (2003) assumed that electron acceleration is continuous through the jet rather than confined to a shock. Then, the steady-state electron index equals that of the acceleration process (e.g. Kirk et al. 1998). Markoff et al. (2003) do not specify details of this acceleration process. A natural candidate here seems to be the second-order Fermi acceleration in a turbulent medium (e.g. Jones 1994), in which case the electron index is constrained only by $p > 1$. This scenario is possible in principle, but then the acceleration depends on the unknown properties of the accelerating medium and equation (8), determining the high-energy cut-off, no longer applies.

The problems with the energy and shape of the high-energy cut-off are even more severe for the non-thermal Compton model (Georganopoulos et al. 2002). It requires that the product of the seed photon energy and the square of the maximum electron energy be fine-tuned, the high-energy cut-off in the electron distribution very sharp and the seed photon distribution very narrow. The last condition is not fulfilled in any of the models of Georganopoulos et al. (2002), which rely on scattering of either disc or stellar blackbody photons. Furthermore, the X-ray jet size in the model of Cyg X-1 of Georganopoulos et al. (2002) is 10^{11} cm, which is clearly inconsistent with the peak of the power spectrum per logarithm of frequency being at some occasions at $\sim$10 Hz (e.g. Revnivtsev, Gilfanov & Churazov 2000).

As discussed in Section 2, the amplitude of Compton reflection and the Fe Kα flux (Section 6) imply that dense and rather cold material occupies a solid angle of $\Omega \sim \pi$ as viewed from the X-ray source. Smearing of these components (e.g. GCR00; Di Salvo et al. 2001; Frontera et al. 2001a) and their correlation with Γ (Sections 2 and 6) clearly identify the reflector with the accretion disc (Section 5) and imply that most of the X-ray source is within $\sim$30–100 gravitational radii from the BH. On the other hand, the models of Markoff et al. (2001, 2002, 2003) and Georganopoulos et al. (2002) ignore that spectral component.

Yet another piece of evidence against a substantial part of the X-rays being non-thermal is provided by spectral variability. In the case of Cyg X-1, the ASM/BATSE data show a pivot around $\sim$40–50 keV (Z02). This is consistent with both the X-ray hardness-flux data and the rms variability strongly increasing with decreasing X-ray energy, see Table 1 and Fig. 9, respectively. The characteristic Δ_Γ from those data is $\sim$0.2–0.3. This power-law spectral variability when extended to the turnover energy (when the synchrotron source becomes optically thick) at $\sim$1 eV (e.g. Markoff et al. 2001, 2003) would imply variability below this energy by a factor of $\sim 10^2$. However, the range of the variability of the 15-GHz flux correlated with the ASM flux in Cyg X-1 is only by a factor of several, basically the same as the range of the variability of the ASM flux itself (Gallo et al. 2002), contradicting the synchrotron origin of X-rays.

If both radio and X-rays were indeed due to non-thermal synchrotron emission (Markoff et al. 2001, 2002, 2003), their observed variability pattern should yield the X-ray rms virtually independent of energy. Then, in the model with non-thermal Comptonization of photons from the companion star (Georganopoulos et al. 2002), the seed photon flux is just constant, and the fractional variability should increase with photon energy globally. These model predictions are in strong disagreement with the data shown in Fig. 9, and,

in particular, with the ASM 1.5–3 keV flux being strongly anticorrelated with the 100–300 keV flux from BATSE (Z02). A similar anticorrelation occurs in Cyg X-3 (McCollough et al. 1999b), and, in fact, the BATSE flux in that object is anticorrelated with radio flux (McCollough et al. 1999a).

On the other hand, if we extrapolate the rms dependence of Fig. 9 to low energies and make a plausible assumption of the fractional rms being <1, we obtain the characteristic energy of a fraction of a keV. This is in very good agreement with the temperature of seed photons for thermal Comptonization observed in Cyg X-1 being $kT_{\rm bb} \sim 0.15$ keV (Ebisawa et al. 1996; Di Salvo et al. 2001).

All of these results strongly support the interpretation of the correlated radio emission being due to ejection of clouds from the X-ray source, which could be similar to coronal mass ejections observed at the Sun. This interpretation is also supported by observed time lags of the radio emission with respect to the X-rays, for example, in GRS 1915+105 (Mirabel et al. 1998). In fact, the base of the jet may be just the hot inner flow (e.g. Fender 2002). However, the electron distribution in that base is still thermal, as argued above.

Finally, we note a problem with internal consistency in the X-ray jet model of GRS 1915+105 of Vadawale et al. (2001). Namely, integrating the model non-thermal synchrotron emission shown in their fig. 4 yields a total jet luminosity of $\sim 10^{41}$ erg s^{-1} (at a distance of 12 kpc, jet velocity of $0.9c$ and $i = 70^\circ$ adopted in that paper; note that this emission is beamed away from the observer). On the other hand, the total jet power given in that paper is 4.3×10^{39} erg s^{-1}. This power includes the proton rest mass, and at the velocity of $0.9c$, the kinetic power is $\sim 2 \times 10^{39}$ erg s^{-1}. Thus, the jet radiative luminosity is $\sim$50 times the kinetic power, which strongly violates energy conservation. Also, the radiative luminosity is usually much less than the kinetic power (unless the jet stops entirely, in which case only the two luminosities can be comparable), which also increases the energy conservation problem.

5 THEORETICAL INTERPRETATION

5.1 Feedback between cold and hot media

The Γ–F and Ω–Γ correlations probably occur as a result of the interaction between cold and hot media. The former correlation (also manifesting itself as pivoting) is probably caused by variability in the flux/luminosity of seed soft photons (emitted by some cold medium) irradiating a hot plasma being much stronger than the variability of the flux/luminosity from the hot plasma itself. The main radiative process in the hot plasma needs to be thermal Compton upscattering of the soft photons. Then, the larger the irradiating flux of seed photons, the softer and stronger the X-ray spectrum. This variability pattern in the case of a constant hot-plasma luminosity is shown, for example, in fig. 3 of ZG01 and fig. 14 of Z02. The pivot point is then somewhere in the middle of the broad-band spectrum. If the hot-plasma luminosity increases as well but slower than the irradiating flux, the pivot is at high energies.

The emission of the cold medium irradiating the hot plasma may be partly (or wholly) due to reprocessing of the emission of the hot plasma. Then, the increased cooling of the hot plasma (which softens the X-ray spectrum) is associated with more Compton reflection (accompanying reprocessing by a Thomson-thick medium). This gives rise to an Ω–Γ correlation (ZLS99; CGR00).

The two patterns can occur together or independently. If the variability of soft seed photons is intrinsic (not from reprocessing), a Γ–F correlation will not be accompanied by an Ω–Γ one. This may happen in narrow-line Seyfert 1s. On the other hand, the variable seed photons may be due to reprocessing but from emission of a highly variable hot plasma. Then, there will be an Ω–Γ correlation but not a Γ–F one, which is the case for, for example, Cyg X-1 on intermediate time-scales (Gilfanov et al., in preparation).

A number of specific geometries have been proposed. In one, there is a variable radial overlap between the hot and cold accretion discs (ZLS99; Poutanen, Krolik & Ryde 1997). In another, the cold disc extends all the way to the minimum stable orbit and the hot plasma forms a corona with a mildly relativistic velocity directed either away from the disc or towards it (Beloborodov 1999a, 2001; Malzac et al. 2001). Also, static coronae have been considered in the context of spectral correlations (e.g. Haardt, Maraschi & Ghisellini 1997; MF01).

5.1.1 *Variable overlap between hot and cold flows*

ZLS99 have interpreted the Ω–Γ correlation as being due to feedback in an inner hot (thermal) accretion flow surrounded by an overlapping cold disc. Then, the closer to the central BH the cold disc extends, the more cooling of the hot plasma by blackbody photons (both reprocessed and from intrinsic dissipation), and the softer the spectrum. The effect of the cooling by the ultraviolet (UV) photons of the X-ray-emitting plasma is seen, for example, in NGC 7469, where there is a positive correlation between the UV flux and Γ (N00). Also, the Γ–F correlation (Section 3) indicates the dominant effect of plasma cooling by a variable seed-photon flux. At the same time, the cold disc subtends a larger solid angle from the point of view of the hot plasma, and thus there are more reflection photons in the spectrum. The solid curve in Fig. 1 shows the prediction of a simple version of this model (ZLS99).

This model also naturally accounts for the correlations of the reflection strength with both the QPO frequency and the degree of relativistic smearing seen in BH binaries (Gilfanov et al. 1999; GCR00; Revnivtsev et al. 2001). The correlation with the QPO frequency is expected because that frequency is very likely to be related in some way to the Keplerian frequency at the inner edge of the cold disc, which increases with the decreasing disc inner radius. At the same time, the closer the reflecting medium is to the BH the higher the degree of the relativistic smearing.

The model naturally explains the pivoting behaviour of the X-ray spectra (manifesting itself in X-rays as a Γ–F correlation) as driven by the variable flux of irradiating seed photons (ZG01; Z02). Also, the specific Γ–F correlations observed in many accreting BHs indicate that the bolometric luminosity increases in those sources with increasing Γ (Section 3). This scenario can account for this behaviour if the inner radius of the cold disc decreases with the increasing accretion rate. Such a behaviour is indeed postulated in models of advection-dominated accretion (e.g. Esin, McClintock & Narayan 1997) and is predicted by models of accretion disc evaporation (Meyer, Liu & Meyer-Hofmeister 2000; Różańska & Czerny 2000). On the other hand, it also appears likely that some instabilities can affect the disc truncation radius even if the bolometric luminosity remains approximately constant, which is observed in some objects (see Section 3).

Chiang & Blaes (2001, 2003) and Chiang (2002) have shown that detailed versions of this model can also explain the overall optical/UV/X-ray variability in a few Seyferts (NGC 3516, 5548, 7469). Note that their calculations require the variable overlap to be mostly achieved by the radius of the hot plasma being variable.

We note that this model does not readily explain $\Omega/2\pi > 1$ sometimes observed (see Figs 1, 3, 4a). Furthermore, scattering of the reflected photons in the hot flow will further reduce the observed Ω (see a discussion in Beloborodov 2001). These problems can possibly be resolved by anisotropy of the emission of the hot plasma or the outer disc being concave. It is also possible that detections of such large reflection are due to imperfection of the spectral models used and/or data inaccuracies.

Within the framework of this model, radio emission arises from outflows in the hot inner flow (e.g. Blandford & Begelman 1999). Such a scenario is described, for example, in Fender (2002). Note that the jet emission in BH binaries is usually quenched in the soft state (Brocksopp et al. 1999; Corbel et al. 2000), in which the hot inner flow most likely disappears and is replaced by a hot corona (e.g. Gierliński et al. 1999).

5.1.2 *Static coronae*

Haardt et al. (1997) have studied spectral correlations in a static disc corona model. They found that if the corona is dominated by $e^{\pm}$ pairs, the 2–10 keV spectral index, Γ is rather insensitive to changes of the flux in the same energy range, with typical $\Delta\Gamma \sim 0.2$ for a change of the flux by 10. This is clearly much less than the observed spectral variability in many sources (Section 3), which rules out this model. The predictions for coronae not dominated by pairs depend, in turn, on the choice of the coronal optical depth, τ. At $\tau \gtrsim 0.3$, Γ would decrease with the flux, contrary to the data, but coronae with lower τ could be reconciled with the data.

Then, MF01 found that static patchy coronae could reproduce the observed Γ–F correlations if the luminosity of an active region increases with its increasing size at a given height. The increased size increases the feedback of soft radiation from the disc, which, in turn, makes the spectrum softer. MF01 and Shih et al. (2002) have shown that this model fits the Γ–F data well for MCG–6-30-15 from *RXTE* and *ASCA*, respectively.

On the other hand, this model yields an Ω–Γ anticorrelation rather than a correlation because an increased size at a given height (leading to the softening of the spectrum, see above) increases the degree of obscuration of the reflected radiation (Beloborodov 1999b; Malzac et al. 2001). This property is also shared by static disc coronae in general, and it follows from the dependences shown by Haardt et al. (1997). Also, static coronae cannot by themselves explain the formation of radio jets.

5.1.3 *Dynamic coronae*

An interpretation of the Ω–Γ correlation alternative to the variable overlap of two accretion flows (Section 5.1.1) is that with mildly relativistic coronal inflows/outflows (Beloborodov 1999a; Malzac et al. 2001). The higher the speed of the coronal outflow, the less feedback with the underlying disc and the harder the spectrum. Inflows can, in turn, account for $\Omega/2\pi > 1$.

It is not clear how to account for the Γ–F correlation in this model. This correlation requires that the observed luminosity of the hot plasma either stays constant or increases with a decrease of the outflow velocity. On the other hand, the opposite behaviour of constant luminosity of the seed photons and variable luminosity of the hot plasma (which results in a Γ–F anticorrelation) is seen in the soft state of Cyg X-1 (Churazov, Gilfanov & Revnivtsev 2001; Z02), in which case coronal models are widely accepted (e.g. Poutanen et al. 1997; Gierliński et al. 1999; Churazov et al. 2001).

Within the framework of this model, radio emission may arise from the jet being formed by the coronal outflow (Merloni & Fabian 2002). However, the quenching of the radio emission in the soft state (Brocksopp et al. 1999; Corbel et al. 2000) is not readily explained in this model.

5.1.4 *Further physical implications*

The feedback models explain the Ω–Γ correlation in terms of Comptonization of blackbody photons by a hot thermal plasma. The effective reflection solid angle in this model can be linked to the geometry of the source, which will also determine the amplification factor, A, of the Comptonization process. On the other hand, the spectral index follows from the energy (and $e^{\pm}$ pair) balance. Since the characteristic blackbody seed photon energy is much lower in AGNs than in BH binaries, a generic prediction of these models is that for a given Ω the value of Γ will be higher in AGNs than that in BH binaries (Beloborodov 1999b; Malzac et al. 2001). This is illustrated in Fig. 10 (for which calculations were performed using the code of Coppi 1999). When the plasma compactness ($\propto L/R$, where L and R are the luminosity and size, respectively), is low, $e^{\pm}$ pair production is negligible and the energy balance is satisfied by adjusting the electron temperature, kT, see Fig. 10(a). On the other hand, at high compactness, the energy balance is achieved by adjusting the Thomson optical depth of the pairs, see Fig. 10(b). (In the calculations shown in Fig. 10b, we assumed the presence of a weak high-energy power-law tail, containing 0.05 of the total $e^{\pm}$ energy beyond the Maxwellian electron distribution, as suggested

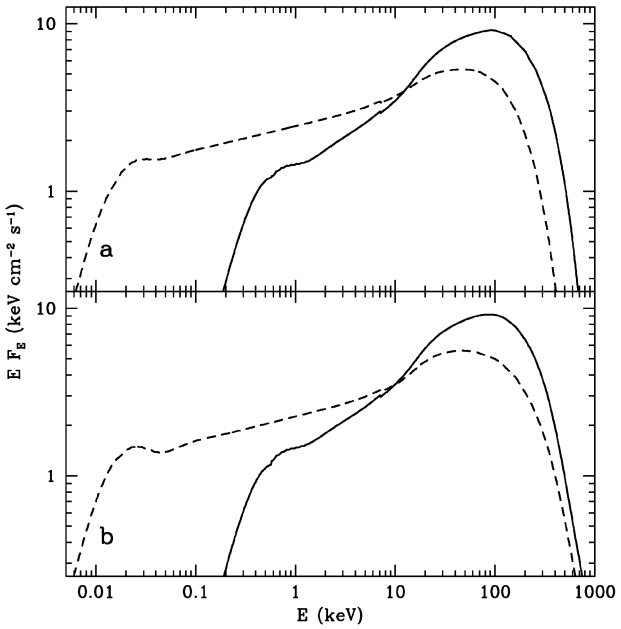

Figure 10. Illustration of the effect of changing $kT_{\rm bb}$ of the seed photons from 5 eV (dashed curves; characteristic to AGNs) to 150 eV (solid curves, characteristic to BH binaries). In both cases the Comptonization amplification factor, $A = 10$. The plasma is dominated by (a) electrons and protons (e^-p) and (b) $e^{\pm}$ pairs. The e^-p plasma parameters are $\tau = 1.5$, $kT = 57$ keV and $\tau = 1.5$, $kT = 87$ keV, in the AGN and BH binary cases, respectively, which yields the corresponding 2–10 keV spectral indices of $\Gamma = 1.85$ and 1.63. The $e^{\pm}$ plasma parameters are $\tau = 1.0$, $kT = 84$ keV and $\tau = 1.6$, $kT = 72$ keV, in the AGN and BH binary cases, respectively. In all cases, $\Omega/2\pi = 0.4$ at $i = 30°$.

by the results of McConnell et al. 2002.) The calculations shown in Fig. 10, with Γ changing from 1.63 to 1.85 at the assumed $\Omega/2\pi = 0.4$, explain well the difference between the Γ–Ω correlations for the BH binaries (Fig. 1) and AGNs (Fig. 3).

An important issue here is also the possible presence of a correlation between Γ and kT for a given $kT_{\rm bb}$. The feedback models require that the parameters of the hot thermal plasma adjust to variable cooling to satisfy the energy balance. If τ is constant, this can be achieved only by changing kT. Then, an increased cooling yielding an increase of Γ is associated with a decrease of kT. On the other hand, it is possible that τ also changes, for example, responding to a changing accretion rate, which would produce a more complicated behaviour (e.g. Chiang & Blaes 2001, 2003). Also, if $e^{\pm}$ pairs are present, the main adjusting parameter is τ. In fact, in the example in Fig. 10(b), the softening of the spectrum is associated with an increase (rather than a decrease) of kT.

So far there are only limited observational data on the correlation between Γ and the high-energy cut-off. P02b found a positive correlation between Γ and the e-folding energy in their sample of Seyfert 1s, which would be contrary to expectations of the simplest model with constant τ and the variability of Γ due to changing kT. However, MP02 found that this correlation may be an artefact of the e-folded power-law model when used to fit thermal-Compton spectra. They simulated actual thermal Comptonization spectra at a *constant* $kT = 100$ keV and a range of τ, and then found that the simulated spectra when fitted by an e-folded power law yield a correlation resembling that of P02b.

5.2 Reflection from strongly ionized disc

Done & Nayakshin (2001) have shown that the optical depth of a highly ionized surface layer on top of a strongly irradiated accretion disc increases with the increasing hardness of the irradiating spectrum. This gives rise to an apparent Ω–Γ correlation as there is less unscattered reflection for harder spectra (although the actual reflection solid angle is $\Omega = 2\pi =$ constant). A separate mechanism is then needed to account for the Γ–F correlation, similarly to the case of the coronal outflow model.

A diagnostic that could yield the actual solid angle of the reflector regardless of the ionization level is a measurement of reflection at high energies. Namely, the reflection spectrum is cut-off at high energies with a functional form independent of the ionization state (White, Lightman & Zdziarski 1988). Fig. 11 illustrates this point for an incident spectrum from Comptonization (Poutanen & Svensson 1996) with $kT = 120$ keV and $\tau = 2$ in spherical geometry, yielding the 2–10 keV index of $\Gamma = 1.5$. This Γ corresponds to the case with the lowest fitted neutral reflection from a strongly ionized medium with the actual $\Omega/2\pi = 1$ in Done & Nayakshin (2001). To illustrate this effect, we assumed that the reflecting medium is so strongly ionized that virtually no Fe K edge appears in the reflection component (the dotted curve in Fig. 11). Although the reflected component is simply a power law at low energies, it still does have a high-energy cut-off due to Klein–Nishina effects. The solid curve shows the total spectrum. Then, the dashed curve shows the incident spectrum without reflection normalized to coincide with the spectrum from the strongly ionized medium. We see that although the spectra at $\lesssim$20 keV are indeed barely distinguishable, the form of their high-energy cutoffs is very different. Thus, this model can be tested using broad-band Xγ spectra extending to several hundred keV.

A set of ~1–1000 keV spectra of Cyg X-1 in the hard state was analysed by Gierliński et al. (1997), who found the form of the high-energy cut-off to be compatible with thermal Comptonization. Although those authors have not consider the ionized-reflection model, the spectra have not shown any hint of the softening of the cut-off of the type seen in the solid curve in Fig. 11; rather they indicated some additional hardening (interpreted by them as being due to the presence of an additional spectral component from saturated Comptonization).

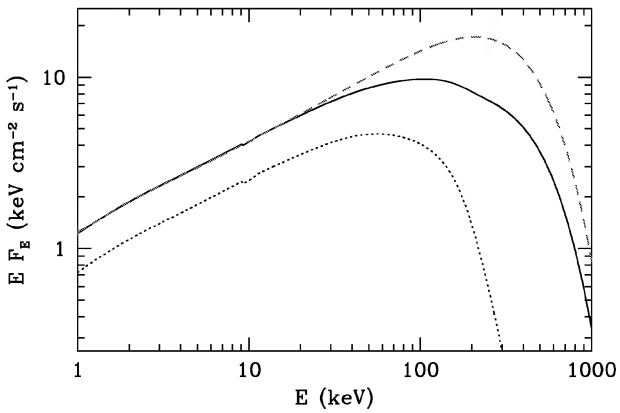

Figure 11. Comptonization spectrum with negligible reflection (dashed curve) compared with a spectrum with $\Omega/2\pi = 1$ and the reflecting medium being almost fully ionized (solid curve). The dotted curve shows the ionized reflection component alone. We see that the form of the high-energy cut-off in the reflection spectral component leads to the total spectrum being distinctly different from the Comptonization spectrum alone (although the two coincide at low energies). See Section 5.2 for details.

Independently of the present work, Barrio, Done & Nayakshin (2003) have recently fitted the ionized reflection model to broad-band spectral data from the PCA and HEXTE detectors of *RXTE* for Cyg X-1. They have found this model to be ruled out by the lack of a break in the HEXTE data, in favour of the model with a truncated disc and intrinsically weak reflection. Future tests of this model are highly desirable, for example, using data from *INTEGRAL* and *ASTRO-E2*.

The effect shown in Fig. 11 also demonstrates that the albedo, a, of a fully ionized medium energy-integrated over a spectrum characteristic to accreting BHs is still substantially less than unity (see also White et al. 1988). Indeed, in the specific case in Fig. 11, $a = 0.48$, only moderately larger than the corresponding albedo for a neutral reflector, $a = 0.34$. This shows that a fully ionized surface layer of an accretion disc would radiate substantial soft thermal flux even in the absence of an internal dissipation. This may rule out the ionized-disc model of the hard state of Cyg X-1 of Young et al. (2001). In general, the resulting constraints on the geometry will be relatively similar to those in the case of a nearly neutral disc (e.g. Stern et al. 1995), and, in particular, will still rule out the presence of a homogeneous corona above the disc.

5.3 Time lags and reflection

N00 have pointed out that the presence of a constant reflection component from a distant medium (presumably a molecular torus) in AGNs together with a variable power law (from hot plasmas in the vicinity of the BH) can lead to an apparent correlation between Γ and Ω if reflection in the fitted model is tied to the variable power law. In particular, when the power law varies with a characteristic pivot energy of $\lesssim$10 keV, the fitted Ω–Γ dependence will be positive

(i.e. the softer the spectrum, the larger the relative contribution of reflection), as illustrated in Fig. 8(a).

This idea has been developed in detail by MP02. They have considered cases with pivot energies of 2, 5 and 10 keV, and have shown that the Ω–Γ dependence in Seyferts (Fig. 3) can be qualitatively explained by this type of model. However, we have shown in Section 3 that the pivot energy in many Seyferts is $\gtrsim$100 keV. Then, if this effect were important for a large fraction of Seyferts, an Ω–Γ *anticorrelation* (see Fig. 8b) would be observed for a large fraction of sources, in conflict with the data. This rules out the origin of the global Ω–Γ dependence in Seyferts from this effect. On the other hand, this effect may be important in some Seyferts, and may explain Ω–Γ anticorrelation in repeated observations of certain objects (Done et al. 2000; P02a).

As noted by MP02, this effect cannot play any role in BH binaries. Thus, this model requires a completely different origin for the Ω–Γ correlations in those objects and in AGNs.

6 THE Fe Kα EMISSION

The results presented in Section 2 were mostly obtained by fits to the Compton-reflection continuum. However, the process of bound–free absorption in the reflecting medium is usually followed by emission of a fluorescent Fe Kα line, for which the equivalent width, $W_{\rm K\alpha}$, can be tied to that of the reflection (George & Fabian 1991; Życki & Czerny 1994). Conversely, if relativistic broadening is seen in the line emitted by the reflecting medium, the same broadening should be seen in the reflection spectrum. Thus, the measured parameters of the Fe Kα line should be in agreement with those of reflection. Such an agreement appears to be seen in BH binaries (Gilfanov et al. 1999; GCR00; Revnivtsev et al. 2001). Some disagreement in GX 339–4 claimed by Nowak et al. (2002) appears to be largely caused by a diffuse line component from the interstellar medium dominating in X-ray weak states of this source (Wardziński et al. 2002).

On the other hand, the situation is more complex in Seyferts. Unlike BH binaries, Seyferts possess a significant Fe Kα line component from distant matter, for example, the broad-line regions or molecular tori. Often, that distant matter is Thomson thin, and then it gives rise to the line but not to an Fe K edge (see, for example, Section 7.1 and fig. 13 in Woźniak et al. 1998). As shown in that figure, the optically thin reflection component is then relatively negligible. Then, the presence of two line components, one constant (with or without associated reflection) and one variable in addition to a variable intrinsic component may cause a rather complex behaviour of variability. For example, the presence of constant line and reflection and a power law pivoting at $\sim$10 keV leads to an anticorrelation of $W_{\rm K\alpha}$ and $\Omega/2\pi$ measured with respect to the power law (see Fig. 8a, also MP02). Such an effect might have been seen by Chiang et al. (2000) in NGC 5548.

Given this complexity, it is important to self-consistently account for various components of the line and reflection, their relativistic broadening, and their connection to the incident spectral component. A self-consistent treatment should in general include at least two line components, narrow and broad, with the broadening (e.g. Gaussian or disc-like) and redshift of the latter applied in the same way to the reflection (e.g., Życki et al. 1998, 1999; GCR00; Lubiński & Zdziarski 2001; Zdziarski et al. 2002a). The strength of reflection should then be tied to that of the line (George & Fabian 1991; Życki & Czerny 1994). The dramatic effect of an inconsistent treatment of the line and reflection is shown for the case of the disc broadening (Fabian et al. 1989) in fig. 3 of Zdziarski et al. (2002a).

Then, Shih et al. (2002) showed that the Fe Kα line flux in MCG–6-30-15 remained approximately constant with varying 3–10 keV *ASCA* count rate. However, the formation of the line is due to photons only above 7.1 keV or more. In the case of MCG–6-30-15, $\Gamma\sim2$, and then the fraction of the measured *ASCA* counts above 7 keV in their data is only $\sim$0.03. The fraction of counts above 8 keV, appropriate for a moderately ionized disc, possibly present in MCG–6-30-15 (e.g. Ballantyne & Fabian 2001), is as low as $\sim$0.01. Thus, the lack of a correlation between the 3–10 keV counts and the line photon flux cannot be taken as conclusive evidence against the Fe Kα photons being due to irradiation by photons from the observed continuum. Similarly, the fraction of counts above 7 and 8 keV in the MCG–6-30-15 data of VE01 is only $\sim$0.2 and $\sim$0.1, respectively. The data of VE01 imply a pivot energy at approximately 80 keV (Table 1); thus, the variability of the flux above $\sim$7–8 keV will, in general, be less than that in the 2–10 keV band used by them (as also found by Markowitz & Edelson 2001 for Seyfert 1s in general).

As noted in Section 3 (and by MP02), there are many AGNs with the pivot at $\lesssim$10 keV (e.g. 3C 120). Then, the 7–10 keV photon flux may be anticorrelated with the 2–10 keV one. Even if the pivot energy is in general at $\gg$10 keV, occasionally the same object may show a pivot at $\lesssim$10 keV, as in the case of NGC 5548 (Nicastro et al. 2000). Thus, it is important to use the band above the Fe K edge in studies of the continuum-line correlations.

Self-consistent treatments of the line and reflection were applied, for example, to the Seyfert galaxy IC 4329A by Done et al. (2000), who found no disagreement between the line and reflection. A similar method was applied to NGC 4151 by Zdziarski et al. (2002a), who also found the broad-line component compatible with reflection, in spite of previous claims to the contrary (e.g. Wang, Zhou & Wang 1999). Then, Lubiński & Zdziarski (2001) have applied the same method to average *ASCA* spectra of Seyfert 1s and found the dependence of the $W_{\rm K\alpha}$ of the broad component of Fe Kα lines to obey the dependence on Γ compatible with that of the reflection continuum. Although Yaqoob et al. (2002) have pointed out that the statistical weights used by Lubiński & Zdziarski (2001) were not justified statistically, the effect of their correction appears to be only minor (Lubiński, in preparation). Indeed, the results of P02b for Seyfert 1s observed by *BeppoSAX* show an increase of $W_{\rm K\alpha}$ with Γ very similar to that obtained by Lubiński & Zdziarski (2001).

7 CONCLUSIONS

We have considered correlations between various spectral properties of accreting BHs in Seyfert galaxies and X-ray binaries, with particular emphasis on the correlations between the X-ray spectral index, the strength of Compton reflection and the X-ray flux. The main results can be summarized as follows.

Using published data of the observations of Seyferts with *Ginga*, *RXTE* and *BeppoSAX*, we have critically re-evaluated the evidence for presence of correlation between the X-ray spectral index and the strength of Compton reflection. We conclude that when considering a large number of observations of a large sample of objects, the existence of a *global* correlation between these two parameters is established beyond any reasonable doubt.

The smallness of the error bars in comparison with the extent of the correlation and good agreement of the results obtained by various satellites confirm that the correlation cannot be an artefact caused by statistical or systematic effects. The ratios of the spectra with different values of reflection in BH binaries demonstrate that the correlation cannot be a consequence of a trivially inadequate spectral model. We note, however, that the particular values of the spectral

index and, especially, of the strength of the Compton reflection, do depend on the details of the spectral approximation. This fact should taken into consideration when comparing results obtained by different authors.

The Ω–Γ correlation shows a significant spread, larger than the statistical uncertainties of the data. It is not clear at present to what degree this spread is intrinsic to the sources and to what degree it is due to imperfection of the spectral model and/or difference in the details of the spectral approximation.

A distinction should be made between classes of objects and multiple observations of individual objects. In the case of luminous BH binaries, the spectral variability of individual sources obeys the general Ω–Γ correlation obtained for BH binaries as a class. In the case of Seyfert galaxies, the correlations hold for a class of objects but can be violated for repeated observations of individual objects, remaining, however, within the spread of the global correlation. In our opinion, these results are still inconclusive and require further investigation as a number of complications are involved in the case of Seyfert galaxies in comparison with X-ray binaries. The most obvious among those are lower statistics due to the significantly lower brightness of Seyferts and the existence of molecular tori and broad line regions, which can give an additional contribution to the reflected component, and uncorrelated with the Comptonized emission on short time-scales.

The physical interpretation of the Ω–Γ and Γ–F correlations will advance our understanding of the geometry of the accretion flow in X-ray binaries and Seyfert galaxies and impose valuable constraints on the theoretical models. At present, the correlations appear to be a natural consequence of co-existence of cold media (e.g. an accretion disc) and a hot Comptonizing cloud in the vicinity of the BH. Their geometrical closeness results in double feedback between the two components of the accretion flow. The cold medium provides seed soft photons for the Comptonization and it reprocesses and reflects the hard radiation from the hot plasma. If a significant fraction of soft seed photons is due to reprocessing of the hard radiation of the hot cloud, furthermore reprocessing results in more cooling of the hot plasma and, correspondingly, in softer X-ray spectra. Among the several specific geometries proposed, the most promising appears to be the disc-spheroid model with variable overlap between the hot and cold components of the accretion flow.

Since the characteristic temperature of the accretion disc in AGNs is much lower than in BH binaries, a generic prediction of this type of models is that for a given value of reflection the value of the spectral index will be higher in AGNs than in BH binaries. This prediction is in good agreement with the observed behaviour.

We presented a diagnostic to test an interpretation of the Ω–Γ correlation as being due to strong ionization of the disc surface layer. It utilizes the independence of the Klein–Nishina cut-off in the reflected spectrum of the ionization state. Applied to existing data, this diagnostic does not support that interpretation.

We found that the pattern of broad-band spectral variability of Seyfert galaxies on a day-to-month time-scale includes a pivoting of a power-law spectrum with the pivot being at a high energy, usually above a few hundred keV. The pivoting explains well the linear correlations between the logarithm of the X-ray flux and Γ seen in both BH binaries and Seyferts. Then, the observed high pivot energies rule out the interpretation of the Ω–Γ correlation in Seyferts being due to a time-lag effect.

We also discuss the correlation between X-ray and radio fluxes in BH binaries and its physical implications. We conclude that this correlation is most likely due to the relation between the level of X-ray emission and the rate of ejection of radio-emitting clouds forming a compact jet. Although peculiar sources might exist, it seems highly unlikely that the correlation is due to the synchrotron origin of the X-ray emission from BH binaries in general.

ACKNOWLEDGMENTS

This research has been supported by grants from KBN (5P03D00821, 2P03C00619p1,2) and the Foundation for Polish Science. We thank J. Poutanen, P.-O. Petrucci, J. Malzac, H. Falcke, M. Sikora, R. Moderski, S. Markoff and K. Leighly for valuable discussions and/or comments. We also acknowledge the referee for important comments on the original version of this work.

REFERENCES

Arnaud K.A., 1996, in Jacoby G.H., Barnes J., eds, ASP Conf. Series Vol. 101, Astronomical Data Analysis Software and Systems V. Astron. Soc. Pac., San Francisco, p. 17
Ballantyne D.R., Fabian A.C., 2001, MNRAS, 323, 506
Ballantyne D.R., Iwasawa K., Fabian A.C., 2001, MNRAS, 323, 506
Barrio F.E., Done C., Nayakshin S., 2003, MNRAS, in press
Beloborodov A.M., 1999a, ApJ, 510, L123
Beloborodov A.M., 1999b, in Poutanen J., Svensson R., eds, ASP Conf. Ser. Vol. 161, High Energy Processes in Accreting Black Holes. Astron. Soc. Pac., San Francisco, p. 295
Beloborodov A.M., 2001, Adv. Space Res., 28, 411
Bevington P.R., Robinson K.D., 1992, Data Reduction and Error Analysis for the Physical Sciences, 2nd edn. McGraw-Hill, New York
Blandford R.D., Begelman M.C., 1999, MNRAS, 303, L1
Brocksopp C., Fender R.P., Larionov V., Lyuty V.M., Tarasov A.E., Pooley G.G., Paciesas W.S., Roche P., 1999, MNRAS, 309, 1063
Chiang J., 2002, ApJ, 572, 79
Chiang J., Blaes O.M., 2001, ApJ, 557, L15
Chiang J., Blaes O.M., 2003, ApJ, 586, 97
Chiang J., Reynolds C.S., Blaes O.M., Nowak M.A., Murray N., Madejski G.M., Marshall H.L., Magdziarz P., 2000, ApJ, 528, 292
Churazov E., Gilfanov M., Revnivtsev M., 2001, MNRAS, 321, 759
Coppi P.S., 1999, in Poutanen J., Svensson R., eds, ASP Conf. Ser. Vol. 161, High Energy Processes in Accreting Black Holes. Astron. Soc. Pac., San Francisco, p. 375
Corbel S., Fender R.P., Tzioumis A.K., Nowak M., McIntyre V., Durouchoux P., Sood R., 2000, A&A, 359, 251
Di Salvo T., Done C., Życki P.T., Burderi L., Robba N.R., 2001, ApJ, 547, 1024
Done C., Nayakshin S., 2001, ApJ, 546, 419
Done C., Mulchaey J.S., Mushotzky R.F., Arnaud K., 1992, ApJ, 395, 275
Done C., Madejski G.M., Życki P.T., 2000, ApJ, 536, 213
Ebisawa K., Ueda Y., Inoue H., Tanaka Y., White N.E., 1996, ApJ, 467, 419
Edelson R., Vaughan S., 2000, BAAS, 32, 416
Eracleous M., Sambruna R., Mushotzky R.F., 2000, ApJ, 537, 654
Esin A.A., McClintock J.E., Narayan R., 1997, ApJ, 489, 865
Fabian A.C., Rees M.J., Stella L., White N.E., 1989, MNRAS, 238, 729
Fender R., 2002, Lecture Notes in Physics, Vol. 589, Relativistic Flows in Astrophysics. Springer-Verlag, Berlin, p. 101
Frontera F. et al., 2001a, ApJ, 546, 1027
Frontera F. et al., 2001b, ApJ, 561, 1006
Gallo E., Fender R., Pooley G.G., 2002, in Durouchoux Ph., Fuchs Y., Rodriguez J., eds, Proc. 4th Microquasar Workshop. Center for Space Physics, Kolkata, p. 201
Georganopoulos M., Aharonian F.A., Kirk J.G., 2002, A&A, 388, L25
George I.M., Fabian A.C., 1991, MNRAS, 249, 352
Gierliński M., 2000, PhD thesis N. Copernicus Astron. Center, Warsaw
Gierliński M., Zdziarski A. A., Done C., Johnson W.N., Ebisawa K., Ueda Y., Haardt F., Phlips B.F., 1997, MNRAS, 288, 958
Gierliński M., Zdziarski A.A., Poutanen J., Coppi P.S., Ebisawa K., Johnson N.W., 1999, MNRAS, 309, 496

Gilfanov M., Churazov E., Revnivtsev M., 1999, A&A, 352, 182
Gilfanov M., Churazov E., Revnivtsev M., 2000, in Zhao G. et al., eds, Proc. 5th CAS/MPG Workshop on High Energy Astrophysics. Science Technical Press, Beijing, p. 114 (GCR00)
Gliozzi M., Sambruna R.M., Eracleous M., 2003, ApJ, 584, 176
Gondek D., Zdziarski A.A., Johnson W.N., George I.M., McNaron-Brown K., Magdziarz P., Smith D., Gruber D.E., 1996, MNRAS, 282, 646
Grandi P., Maraschi L., Urry C.M., Matt G., 2001, ApJ, 556, 35
Grove J.E., Johnson W.N., Kroeger R.A., McNaron-Brown K., Skibo J.G., 1998, ApJ, 500, 899
Haardt F., Maraschi L., Ghisellini G., 1997, ApJ, 476, 620
Johnson W.N., McNaron-Brown K., Kurfess J.D., Zdziarski A.A., Magdziarz P., Gehrels N., 1997, ApJ, 482, 173
Jones F.C., 1994, ApJS, 90, 561
Kirk J.G., Rieger F.M., Mastichiadis A., 1998, A&A, 333, 452
Kotov O., Churazov E., Gilfanov M., 2001, MNRAS, 327, 799
Lamer G., McHardy I.M., Uttley P., Jahoda K., 2003, MNRAS, 338, 323
Lee J.C., Fabian A.C., Reynolds C.S., Iwasawa K., Brandt W.N., 1998, MNRAS, 300, 583
Leighly K.M., 1999, ApJS, 125, 297
Leighly K.M., Mushotzky R.F., Yaqoob T., Kunieda H., Edelson R., 1996, ApJ, 469, 147
Li T.P., Feng Y.X., Chen L., 1999, ApJ, 521, 789
Lightman A.P., White T.R., 1988, ApJ, 335, 57
Lubiński P., Zdziarski A.A., 2001, MNRAS, 323, L37
Madejski G.M., Done C., Życki P., 2001, Adv. Space Res., 28, 369
Magdziarz P., Zdziarski A.A., 1995, MNRAS, 273, 837
Magdziarz P., Blaes O.M., Zdziarski A.A., Johnson W.N., Smith D.A., 1998, MNRAS, 301, 179
Malzac J., Petrucci P.-O., 2002, MNRAS, 336, 1209 (MP02)
Malzac J., Beloborodov A.M., Poutanen J., 2001, MNRAS, 326, 417
Markoff S., Falcke H., Fender R., 2001, A&A, 372, L25
Markoff S., Nowak M., Fender R., Falcke H., 2002, in Durouchoux Ph., Fuchs Y., Rodriguez J., eds, Proc. 4th Microquasar Workshop. Center for Space Physics, Kolkata, p. 140
Markoff S., Nowak M., Corbel S., Falcke H., Fender R., 2003, A&A, 397, 645
Markowitz A., Edelson R., 2001, ApJ, 547, 684
Matt G., 2001, in White N.E., Malaguti G., Palumbo G.G.C., eds, AIP Conf. Proc. 599, X-ray Astronomy. Stellar Endpoints, AGN and the Diffuse X-ray Background. AIP, New York, p. 209
McBreen B., Hurley K.J., Long R., Metcalfe L., MNRAS, 271, 662
McCollough M.L. et al., 1999a, ApJ, 517, 951
McCollough L.M. et al., 1999b, Astrophys. Lett. Commun., 38, 105
McConnell M.L. et al., 2002, ApJ, 572, 984
Merloni A., Fabian A.C., 2001, MNRAS, 328, 958 (MF01)
Merloni A., Fabian A.C., 2002, MNRAS, 332, 165
Meyer F., Liu B.F., Meyer-Hofmeister E., 2000, A&A, 354, L67
Miller J.M., Ballantyne D.R., Fabian A.C., Lewin W.H.G., 2002, MNRAS, 335, 865
Mirabel I.F., Dhawan V., Chaty S., Rodriguez L.F., Marti J., Robinson C.R., Swank J., Geballe T., 1998, A&A, 330, L9
Nandra K., Pounds K.A., 1994, MNRAS, 268, 405
Nandra K., Le T., George I.M., Edelson R.A., Mushotzky R.F., Peterson B.M., Turner T.J., 2000, ApJ, 544, 734 (N00)
Narayan R., Yi I., 1995, ApJ, 452, 710
Nicastro F. et al., 2000, ApJ, 536, 718
Nowak M.A., Wilms J., Dove J.B., 2002, MNRAS, 332, 856
Orr A., Barr P., Guainazzi M., Parmar A.N., Young A.J., 2001, A&A, 376, 413
Page K.L., Pounds K.A., Reeves J.N., O'Brien P.T., 2002, MNRAS, 330, L1
Papadakis I.E., Petrucci P.O., Maraschi L., McHardy I.M., Uttley P., Haardt F., 2002, ApJ, 573, 92 (P02a)
Perola G.C., Matt G., Cappi M., Fiore F., Guainazzi M., Maraschi L., Petrucci P.O., Piro L., 2002, A&A, 389, 802 (P02b)
Pounds K.A., Nandra K., Stewart G.G., George I.M., Fabian A.C., 1990, Nat, 344, 132
Pounds K.A., Done C., Osborne J.P., 1995, MNRAS, 277, L5
Poutanen J., Svensson R., 1996, ApJ, 470, 249
Poutanen J., Zdziarski A.A., 2002, in Durouchoux Ph., Fuchs Y., Rodriguez J., eds, Proc. 4th Microquasar Workshop. Center for Space Physics, Kolkata, p. 87
Poutanen J., Krolik J.H., Ryde F., 1997, MNRAS, 292, L21
Ptak A., Yaqoob T.Y., Serlemitsos P.J., Mushotzky R.F., Otani C., 1994, ApJ, 436, L31
Rau A., Greiner J., 2003, A&A, 397, 711
Revnivtsev M., Gilfanov M., Churazov E., 1999, A&A, 347, L23
Revnivtsev M., Gilfanov M., Churazov E., 2000, A&A, 363, 1013
Revnivtsev M., Gilfanov M., Churazov E., 2001, A&A, 380, 520
Różańska A., Czerny B., 2000, A&A, 360, 1170
Shih D.C., Iwasawa K., Fabian A.C., 2002, MNRAS, 333, 687
Stecker F.W., Salamon M.H., 1996, ApJ, 464, 600
Stern B.E., Poutanen J., Svensson R., Sikora M., Begelman M.C., 1995, ApJ, 449, L13
Ueda Y., Ebisawa K., Done C., 1994, PASJ, 46, 107
Vadawale S.V., Rao A.R., Chakrabarti S.K., 2001, A&A, 372, 793
Vaughan S., Edelson R., 2001, ApJ, 548, 694 (VE01)
Wang J.-X., Zhou Y.-Y., Wang T.-G., 1999, ApJ, 523, L129
Wardziński G., Zdziarski A.A., 2000, MNRAS, 314, 183
Wardziński G., Zdziarski A.A., Gierliński M., Grove J.E., Jahoda K., Johnson W.N., 2002, MNRAS, 337, 829
Weaver K.A., Krolik J.H., Pier E.A., 1998, ApJ, 498, 213
Wen L., Cui W., Bradt H.V., 2001, ApJ, 546, L105
White T.R., Lightman A.P., Zdziarski A.A., 1988, ApJ, 331, 939
Wilms J., Nowak M.A., Dove J.B., Fender R.P., di Matteo T., 1999, ApJ, 522, 460
Woźniak P.R., Zdziarski A.A., Smith D., Madejski G.M., Johnson W.N., 1998, MNRAS, 299, 449
Yaqoob T., Warwick R.S., Makino F., Otani C., Sokoloski J.L., Bond I.A., Yamauchi M., 1993, MNRAS, 262, 435
Yaqoob T., Padmanabhan U., Dotani T., Nandra K., 2002, ApJ, 569, 487
Young A.J., Fabian A.C., Ross R.R., Tanaka Y., 2001, MNRAS, 325, 1045
Zdziarski A.A., 1999, in Poutanen J., Svensson R., eds, ASP Conf. Ser. Vol. 161, High Energy Processes in Accreting Black Holes. Astron. Soc. Pac., San Francisco, p. 16
Zdziarski A.A., Grandi P., 2001, ApJ, 551, 186 (ZG01)
Zdziarski A.A., Johnson W.N., Done C., Smith D., McNaron-Brown K., 1995, ApJ, 438, L63
Zdziarski A.A., Johnson W.N., Magdziarz P., 1996, MNRAS, 283, 193
Zdziarski A.A., Poutanen J., Mikolajewska J., Gierliński M., Ebisawa K., Johnson W.N., 1998, MNRAS, 301, 435
Zdziarski A.A., Lubiński P., Smith D.A., 1999, MNRAS, 303, L11 (ZLS99)
Zdziarski A.A., Poutanen J., Johnson W.N., 2000, ApJ, 542, 703
Zdziarski A.A., Leighly K.M., Matsuoka M., Cappi M, Mihara T., 2002a, ApJ, 573, 505
Zdziarski A.A., Poutanen J., Paciesas W.S., Wen L., 2002b, ApJ, 578, 357 (Z02)
Życki P.T., Czerny B., 1994, MNRAS, 266, 653
Życki P.T., Done C., Smith D.A., 1998, ApJ, 496, L25
Życki P.T., Done C., Smith D.A., 1999, MNRAS, 305, 231

APPENDIX A: PIVOTING

Let us consider spectral variability consisting of pivoting. Namely, an initial spectrum (a power law or not) is multiplied by $(E/E_{\rm p})^{\delta} \equiv f$, where $E_{\rm p}$ is the pivot energy and δ is a perturbation spectral index. In particular, when the initial spectrum is a power law, we have a variable power-law photon spectrum, $\mathrm{d}\dot{N}/\mathrm{d}E = C(E/E_{\rm p})^{-\Gamma}$, where C is a constant. Then there is linear relation between the logarithm of the monochromatic flux at a given energy, E, and the variable slope,

$$\ln(\mathrm{d}\dot{N}/\mathrm{d}E) = \ln(E_{\rm p}/E)\Gamma + \ln C. \qquad \text{(A1)}$$

A similar linear relation holds approximately for the energy flux in an interval from E_1 to E_2. Thus, pivoting results in an (approximate)

linear dependence between the logarithm of the flux (not the flux itself) and the spectral index, as illustrated by the dashed lines in Fig. 7.

A1 Moments of the flux

If pivoting variability occurs on time-scales shorter than a given observation, the measured average spectrum will consist of the initial spectrum (in particular, a power law itself) times the average of f, $\bar{f}$. If E_p =constant and the distribution in time of δ is uniform from $-\Delta_\Gamma$ to $+\Delta_\Gamma$, the flux average is given by

$$\bar{f} = \frac{\sinh x}{x} = 1 + \frac{x^2}{6} + O(x^4), \tag{A2}$$

where

$$x \equiv \Delta_\Gamma \ln(E/E_\mathrm{p}). \tag{A3}$$

If the distribution of δ is Gaussian, i.e. $\propto\exp[-(\delta/\Delta_\Gamma)^2/2]$ (where now Δ_Γ is the standard deviation of the distribution of δ), we have,

$$\bar{f} = \mathrm{e}^{x^2/2} = 1 + \frac{x^2}{2} + O(x^4). \tag{A4}$$

Note that the concave form of these spectra yield strong departures from the initial power law at $E \ll E_\mathrm{p}$. Pivoting on short time-scales can account (at least in part) for the soft X-ray excesses commonly seen in Seyferts and BH binaries. Pivoting may also explain an apparently concave part of the extragalactic γ-ray spectrum (Stecker & Salamon 1996), although it requires the pivot energy to be within that part (this issue was not considered by those authors).

This variability will also contribute to the flux variance, $\sigma^2 = \langle(f-\bar{f})^2\rangle$. The variance normalized to the average flux is given by

$$\frac{\sigma^2}{\bar{f}^2} = x\coth x - 1 = \frac{x^2}{3} + O(x^4), \tag{A5}$$

for the uniform distribution of δ, and

$$\sigma^2 = \mathrm{e}^{2x^2} - \mathrm{e}^{x^2}, \quad \frac{\sigma^2}{\bar{f}^2} = \mathrm{e}^{x^2} - 1 = x^2 + O(x^4), \tag{A6}$$

for the Gaussian distribution of δ. With the addition of some energy-independent variability, σ_0^2, the ratio $(\sigma^2+\sigma_0^2)/\bar{f}^2$ reproduces well the fractional variability of Cyg X-1 in the hard state on long time-scales, see Fig. 9.

Then, the skewness, $s = \langle(f-\bar{f})^3\rangle/\sigma^3$, is given by,

$$s = \frac{6 + x\,[x + 3\,(x\coth x - 3)\coth x]}{3\,(x\coth x - 1)^{3/2}} = \frac{2\sqrt{3}|x|}{5} + O(x^3), \tag{A7}$$

for the uniform distribution of δ, and

$$s = \left(\mathrm{e}^{x^2}-1\right)^{1/2}\left(\mathrm{e}^{x^2}+2\right) = 3|x| + O(x^3), \tag{A8}$$

for the Gaussian distribution of δ. This quantity may be useful for testing whether a given variability pattern is related to pivoting. Also, the kurtosis, $S = \langle(f-\bar{f})^4\rangle/\sigma^4 - 3$, is given by

$$S = \mathrm{e}^{2x^2}\left[\mathrm{e}^{x^2}\left(\mathrm{e}^{x^2}+2\right)+3\right] - 6 = 16x^2 + O(x^4), \tag{A9}$$

for the Gaussian distribution of δ.

On the other hand, it is rather unlikely that the pivot energy is completely constant in an astrophysical system. Instead, a range of pivoting energy is expected from some physical constraints on the emitting plasma, see fig. 3 in ZG01 and fig. 14 in Z02. Therefore, we also consider a case when the pivot energy is distributed log-normally, i.e. given by $\ln E_\mathrm{p} = \ln E_\mathrm{p}^0 - \epsilon$, where ϵ is distributed $\propto\exp[-(\epsilon/\Delta_\mathrm{p})^2/2]$ and Δ_p is the standard deviation of this distribution. When δ is also distributed normally, the average departure from the original spectrum is given by

$$\bar{f} = \frac{\mathrm{e}^{x^2/[2(1-\Delta^2)]}}{(1-\Delta^2)^{1/2}} = \frac{1}{(1-\Delta^2)^{1/2}} + \frac{x^2}{2(1-\Delta^2)^{3/2}} + O(x^4), \tag{A10}$$

where

$$\Delta \equiv \Delta_\Gamma\Delta_\mathrm{p} < 1, \quad x \equiv \Delta_\Gamma \ln\left(E/E_\mathrm{p}^0\right). \tag{A11}$$

The variance is then

$$\sigma^2 = \frac{\mathrm{e}^{2x^2/(1-4\Delta^2)}}{(1-4\Delta^2)^{1/2}} - \frac{\mathrm{e}^{x^2/(1-2\Delta^2)}}{(1-2\Delta^2)^{1/2}} \tag{A12}$$

and the variance normalized to the average flux is

$$\begin{aligned}\frac{\sigma^2}{\bar{f}^2} &= \frac{1-\Delta^2}{\left(1-4\Delta^2\right)^{1/2}}\exp\left[\frac{(1+2\Delta^2)x^2}{(1-4\Delta^2)(1-\Delta^2)}\right] \\ &\quad - \frac{1-\Delta^2}{(1-2\Delta^2)^{1/2}}\exp\left[\frac{\Delta^2x^2}{(1-2\Delta^2)(1-\Delta^2)}\right] \\ &= (1-\Delta^2)\left[(1-4\Delta^2)^{-1/2} - (1-2\Delta^2)^{-1/2}\right] \\ &\quad + \left[\frac{1+2\Delta^2}{(1-4\Delta^2)^{3/2}} - \frac{\Delta^2}{(1-2\Delta^2)^{3/2}}\right]x^2 + O(x^4),\end{aligned} \tag{A13}$$

for $\Delta < \frac{1}{2}$. Note that a finite range of the pivot energy results in a finite variance at $E = E_\mathrm{p}^0$, as given by the third line of equation (A13), in contrast to the case with the fixed pivot, equation (A6). Thus, the above dependence fits well the long-term behaviour of Cyg X-1 in the hard state without an additional constant, see Fig. 9.

The skewness is given by,

$$\begin{aligned}\langle(f-\bar{f})^3\rangle = s\sigma^3 &= \frac{\mathrm{e}^{9x^2/(2-18\Delta^2)}}{(1-9\Delta^2)^{1/2}} + \frac{2\mathrm{e}^{3x^2/(2-6\Delta^2)}}{(1-3\Delta^2)^{1/2}} \\ &\quad - \frac{3\mathrm{e}^{5x^2/(2-10\Delta^2)}}{(1-5\Delta^2)^{1/2}},\end{aligned} \tag{A14}$$

for $\Delta < 1/3$.

Above, we assumed that variations of the pivot energy are uncorrelated with those of the spectral index. Note that a correlation between these quantities would result in time lags between light curves measured at different energies (Kotov, Churazov & Gilfanov 2001).

A2 Moments of the logarithm of flux

The moments of the distributions above assume especially simple forms for the logarithm of flux. We define,

$$g \equiv \ln f = \delta\ln(E/E_\mathrm{p}), \tag{A15}$$

where f is a departure from the initial spectrum, as above. Then, for a Gaussian distribution of δ and a constant E_p, the distribution of g is Gaussian itself, with

$$\bar{g} = 0, \quad \sigma^2 = x^2, \quad s = 0, \quad S = 0. \tag{A16}$$

Thus, the apparently non-Gaussian distribution of the linear flux (equations A8 and A9) becomes completely Gaussian when its logarithm is used. Such lognormal distributions are, in fact, very common in natural phenomena ranging from terrestrial lightning to γ-ray bursts (McBreen et al. 1994). Note then that a positive skewness of the distribution of a linear variable (e.g. Leighly 1999) is

not necessary an indication of non-Gaussianity of the underlying processes.

In the case of Gaussian distributions of both δ and ϵ, g is a product of two variables (δ and ϵ + constant), each having a Gaussian distribution, and

$$\bar{g} = 0, \quad \sigma^2 = \Delta^2 + x^2, \quad s = 0, \quad S = \frac{6\Delta^2(\Delta^2 + 2x^2)}{(\Delta^2 + x^2)^2}. \quad \text{(A17)}$$

Note that σ^2 and S are not simply products of the corresponding quantities for each of the two variables due to a non-zero centre value of the latter. Then, the resulting distribution of g is not completely Gaussian, and, in particular, $S > 0$.

This paper has been typeset from a TEX/LATEX file prepared by the author.